Table 2
S-Nitroso moieties (SNO mol/mol USA) after incubation with GS-NO.

GS-NO incubation time (min)	0	1	15	60
HSA alone	0.00 ± 0.00	0.06 ± 0.03	0.12 ± 0.03	0.31 ± 0.03
HSA with N-AcTrp	0.00 ± 0.00	0.08 ± 0.02	0.13 ± 0.02	0.33 ± 0.06
HSA with CA	0.00 ± 0.00	0.29 ± 0.06**	0.31 ± 0.06**	0.41 ± 0.08**
HSA with CA and N-AcTrp	0.00 ± 0.00	0.42 ± 0.09**	0.45 ± 0.10**	0.51 ± 0.09**
HSA formulation	0.00 ± 0.00	0.35 ± 0.05**	0.41 ± 0.10**	0.45 ± 0.09**

Results are given as means ± SEM (n = 3–10).
** $P < 0.01$, as compared with HSA alone.

viral or other biological agents [11]. We used the solutions from Chemo-Sera-Therapeutic Research Institute as an illustrative example, and this formulation has 5–6 mol of each of the two ligands per mol of HSA. Furthermore, it has a high percentage of mercaptalbumin, i.e. 71 ± 8% (n = 6). Therefore, we investigated whether a simple incubation of the formulation with GS-NO would result in significant amounts of SNO-HSA. As seen from Table 2, this one-step procedure also resulted in an efficient and fast *S*-nitrosation of HSA.

Physicochemical properties and stability of S-nitrosated HSA

According to reduced and non-reduced SDS–PAGE, the one-step *S*-nitrosation of formulation HSA did not result in the formation of dimer via disulfide bond formation, fragmentation or other gross conformational changes (Fig. 4A). Any minor conformational changes were examined for by using circular dichroism spectroscopy. The far-UV spectra (Fig. 4B) and the near-UV spectra (Fig. 4C) show that *S*-nitrosation of Cys-34 had no evident effect on the secondary or tertiary structure of HSA. Previous examinations with non-reducing SDS–PAGE revealed that *S*-nitrosation of defatted, DTT-treated HSA only results in, if any, changes in the tertiary structure of the protein [9]. Thus, our data propose that *S*-nitrosation does not induce significant conformational changes in any of our protein preparations. The stability of SNO-HSA with 5 mol of CA and N-AcTrp per mol of protein was tested in two different ways. First, the half-life of the *S*-nitroso moiety of SNO-HSA with the ligands was 50 days in phosphate buffer, pH 7.4, in the dark. Without the ligands the half-life was only 25 days. Second, lyophilization with CA and N-AcTrp resulted in only a slight decrease (10%) in *S*-nitroso content. Thus, SNO-HSA with CA and N-AcTrp is very stable.

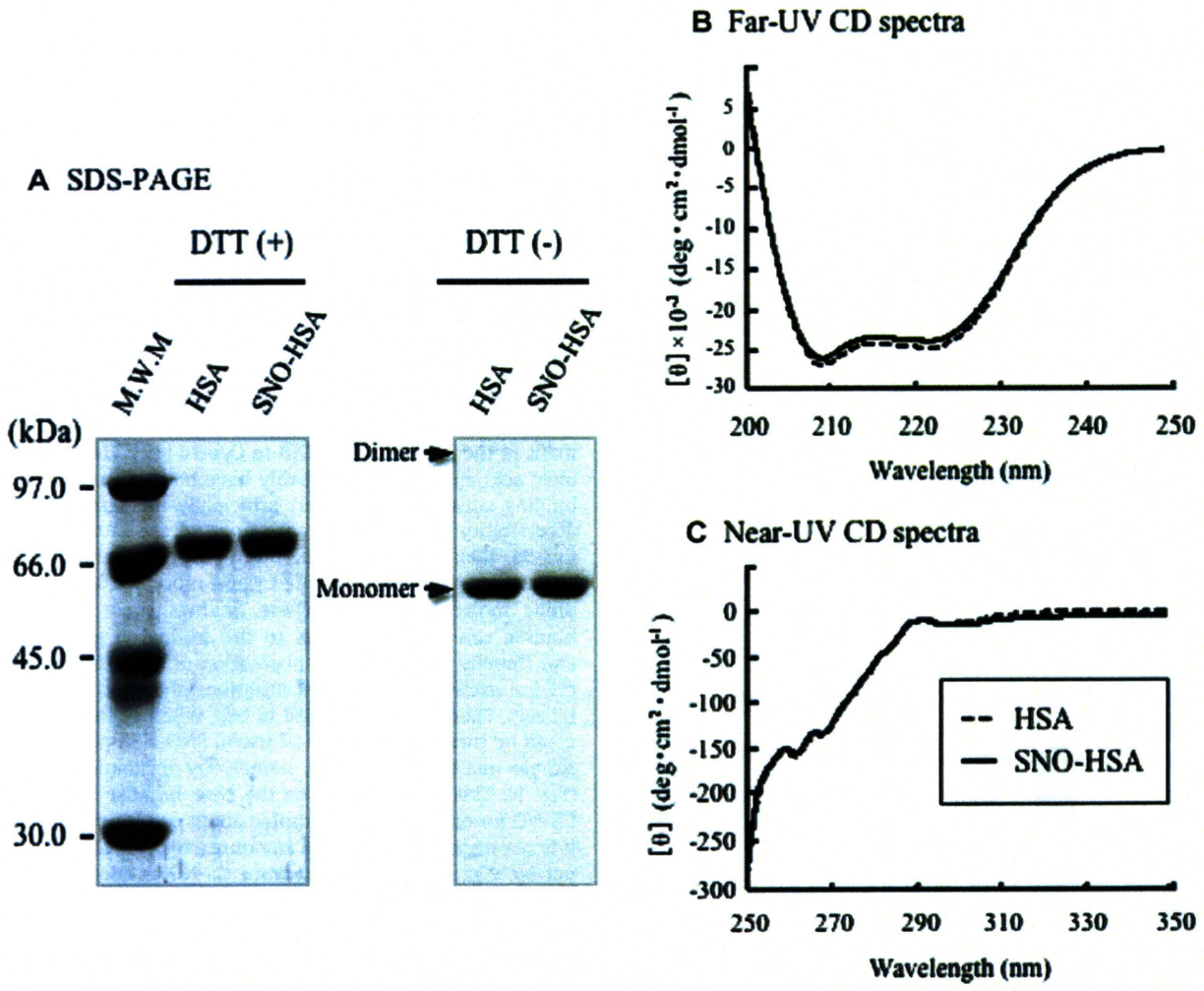

Fig. 4. Structural integrity of HSA and SNO-HSA. (A) Reduced and non-reduced SDS–PAGE of HSA and SNO-HSA. 1 μg of protein was added to each lane, and the gel was stained by CBB. Molecular mass markers are indicated at the left of the gel. B and C show far-UV and near-UV CD spectra, respectively, of HSA and SNO-HSA. The proteins were unmodified and *S*-nitrosated HSA formulation.

Cytoprotective effect of SNO-HSA against ischemia–reperfusion injury

We tested the biological usefulness of the one-step SNO-HSA preparation by studying its cytoprotective effect in an ischemia–reperfusion liver injury model in rats [9,16,20]. Previous studies with SNO-HSA showed that a quantity of 0.1 μmol protein/rat was most suitable for this kind of experiment [9]. Therefore, we used the same quantity of SNO-HSA in this study. To evaluate liver injury, we measured the extracellular release of the liver enzymes ALT and AST via plasma enzyme values. Without adding albumin, the ALT-values increased to a maximum at 1 h after reperfusion. After 2 h the value was slightly lower and then decreased further and gradually during 24 h. Principally the same results were obtained for AST (data not shown). Administration of DTT-treated HSA, of the original HSA formulation or of GS-NO at the beginning of reperfusion did not modify liver damage (Fig. 5A). However, a significant reduction in the release of ALT was observed in rats treated with SNO-HSA, which had been made by incubating defatted, DTT-treated HSA (5 mol CA and N-AcTrp/mol HSA) with GS-NO for 60 min. The same, or even better, cytoprotection was obtained after injecting SNO-HSA, which had been made by incubating the original HSA formulation with GS-NO for only 1 min. Again, principally the same results were obtained for AST (data not shown). We have also determined the expression of the intracellular, cytoprotective enzyme HO-1 in the liver cells 6 h after reperfusion. Fig. 5B shows that if DTT-treated HSA, HSA formulation or GS-NO was injected at the beginning of reperfusion, a pronounced induction of HO-1 took place. However, the most pronounced induction took place after injection of SNO-HSA. As an internal control we determined the amount of β-actin (Fig. 5B). The density of the HO-1 and β-actin bands were quantified and related to each other. Also this type of analysis showed that administration of SNO-HSA resulted in a very pronounced induction of HO-1. The HO-1 expression increased as follows: DTT-treated HSA = HSA formulation < GS-NO < SNO-HSA, which had been made by incubating DTT-treated HSA (5 mol CA and N-AcTrp/mol HSA) with GS-NO for 60 min < SNO-HSA, which had been made by incubating the original HSA formulation with GS-NO for only 1 min. Thus, in addition to *S*-nitrosation, binding of CA and N-AcTrp improved the cytoprotective effect. *S*-Nitrosothiols such as SNO-HSA can exert cytoprotective effects in different ways. In addition to inducing HO-1, the effect can be brought about by, for example, maintenance of tissue blood flow, suppression of neutrophil infiltration and reduction of apoptosis in the liver [16].

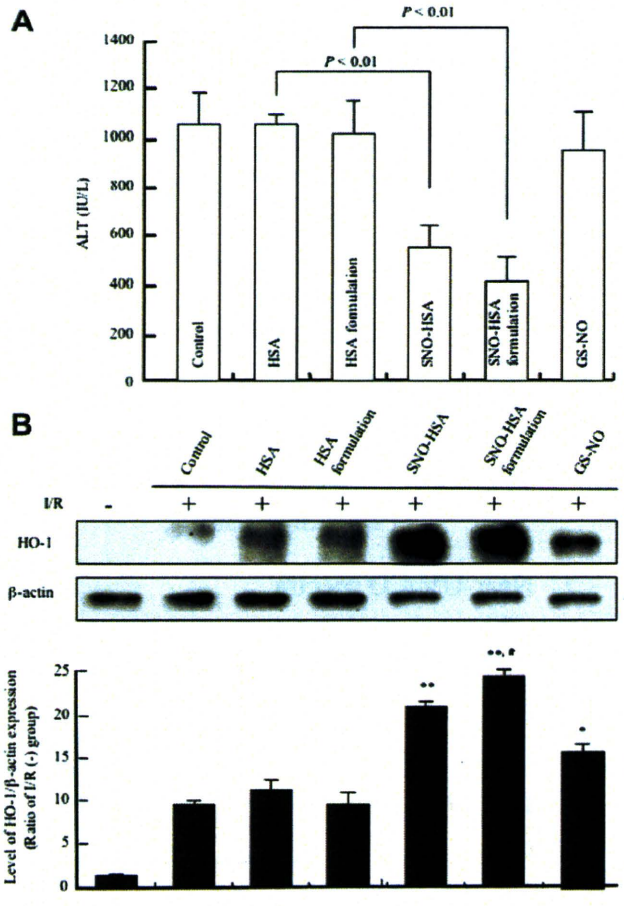

Fig. 5. Serum levels of ALT and Western blot of HO-1 and β-actin in liver cells after hepatic ischemia–reperfusion in rats. (A) Saline (control), HSA, HSA formulation, SNO-HSA, SNO-HSA formulation or GS-NO (the same amount of SNO administration as with SNO-HSA) was injected at the beginning of reperfusion (0 min), and the activities of ALT were measured at 60 min after reperfusion. (B) Western blot of HO-1 and β-actin in liver cells 6 h after hepatic ischemia–reperfusion. I/R (−) are results from rats, which had not been subject to ischemia–reperfusion. The density of the bands for HO-1 and β-actin was quantitatively analyzed using the NIH Image J Software. Data are expressed as means ± SEM ($n = 4$). *, $p < 0.05$, **, $p < 0.01$, compared with I/R (−). #, $p < 0.05$, compared with SNO-HSA.

Discussion

SNO-HSA has been shown to be cytoprotective against free radical mediated damage and microvascular injury associated with ischemia–reperfusion or hemorrhagic shock as well as acute lung injury in a murine model of sickle cell disease. Therefore, SNO-HSA is under investigation as a therapeutic agent in humans. However, existing methods for making SNO-HSA preparations are complicated and time-consuming, see the illustrative overview in Fig. 1. In the first parts of this work, we observed that binding of CA and N-AcTrp resulted in a very pronounced increment in *S*-nitrosation of HSA when incubated with GS-NO. The increment is most probably caused by an easier access of GS-NO to the sulfhydryl group of Cys-34 and protection of the residue against oxidation. In addition, the presence of the ligands resulted in an increased stability of the *S*-nitrosated product. We have previously found that binding of oleic acid resulted in an almost linear increment in the reactivity of DTNB to Cys-34 [12]. Thus, even though oleic acid and CA most probably have both common and private binding sites [21], they exert principally the same effect on the accessibility of Cys-34. Because none of the fatty acids bind to Cys-34, their effects must be due to binding-induced conformational changes of HSA making Cys-34 more accessible to electrophilic molecules [12,14]. These findings show that fatty acid binding can ease the access to the sulfhydryl group of Cys-34 and thereby improve the *S*-nitrosation of HSA. HSA solutions for clinical use contain high concentrations of CA and N-AcTrp as stabilizers. Therefore, we decided to test, whether such formulations could be turned into biological useful SNO-HSA preparations by a simple one-step procedure, namely by incubation with GS-NO (Fig. 1). This was found to be the case, because incubation with GS-NO for only 1 min *S*-nitrosated about one third of the albumin. It is not necessary to remove any unreacted GS-NO from the product by, e.g., gel filtration, because GS-NO is eliminated fast and apparently without secondary effects from the circulation [9]. We tested the biological usefulness of the preparation by studying its cytoprotective effect in an ischemia–reperfusion liver injury model. The results showed that it had a superior biological activity, and that CA and N-AcTrp binding improved the effect. The present findings can probably be of practical use, because instead of giving patients a simple HSA formulation, the formulation can easily and

fast be upgraded to a solution with a high concentration of SNO-HSA, which could be of greater help to the patient and have a broader application. The clinical development of SNO-HSA as a strong cytoprotecting agent is under way using our simple method in collaboration with clinicians of hospital and developers of drug industry.

Acknowledgments

This work was supported in part by Grants-in-Aid from the Japan Society for the Promotion of Science (JSPS), a Grant-in-Aid from the Ministry of Education, Culture, Sports, Science and Technology, Japan (18390051), and by Fonden af 1870. Thanks are also due to members of the Gene Technology Center in Kumamoto University for their important contributions to the experiments.

References

[1] L.J. Ignarro, P.J. Kadowitz, W.H. Baricos, Evidence that regulation of hepatic guanylate cyclase activity involves interactions between catalytic site –SH groups and both substrate and activator, Arch. Biochem. Biophys. 208 (1981) 75–86.
[2] L.J. Ignarro, H. Lippton, J.C. Edwards, W.H. Baricos, A.L. Hyman, P.J. Kadowitz, C.A. Gruetter, Mechanism of vascular smooth muscle relaxation by organic nitrates, nitrites, nitroprusside and nitric oxide: evidence for the involvement of S-nitrosothiols as active intermediates, J. Pharmacol. Exp. Ther. 218 (1981) 739–749.
[3] L.J. Ignarro, B.K. Barry, D.Y. Gruetter, J.C. Edwards, E.H. Ohlstein, C.A. Gruetter, W.H. Baricos, Guanylate cyclase activation of nitroprusside and nitrosoguanidine is related to formation of S-nitrosothiol intermediates, Biochem. Biophys. Res. Commun. 94 (1980) 93–100.
[4] N. Hogg, Biological chemistry and clinical potential of S-nitrosothiols, Free Rad. Biol. Med. 28 (2000) 1478–1486.
[5] M.W. Foster, T.J. McMahon, J.S. Stamler, S-nitrosation in health and disease, Trends Mol. Med. 9 (2003) 160–168.
[6] J.S. Stamler, D.I. Simon, J.A. Osborne, M.E. Mullins, O. Jaraki, T. Michel, D.J. Singel, J. Loscalzo, S-nitrosation of proteins with nitric oxide: synthesis and characterization of biologically active compounds, Proc. Natl. Acad. Sci. USA 89 (1992) 444–448.
[7] S. Hallstrom, H. Gasser, C. Neumayer, A. Fugl, J. Nanobashvili, A. Jakubowski, I. Huk, G. Schlag, T. Malinski, S-nitroso human serum albumin treatment reduces ischemia/reperfusion injury in skeletal muscle via nitric oxide release, Circulation 105 (2002) 3032–3038.
[8] M. Dworschak, M. Franz, S. Hallstrom, S. Semsroth, H. Gasser, M. Haisjackl, B.K. Podesser, T. Malinski, S-nitroso human serum albumin improves oxygen metabolism during reperfusion after severe myocardial ischemia, Pharmacology 72 (2004) 106–112.
[9] Y. Ishima, T. Sawa, U. Kragh-Hansen, Y. Miyamoto, S. Matsushita, T. Akaike, M. Otagiri, S-nitrosylation of human variant albumin Liprizzi (R410C) confers potent antibacterial and cytoprotective properties, J. Pharmacol. Exp. Ther. 320 (2007) 969–977.
[10] T. Peters Jr., All About Albumin: Biochemistry, Genetics, and Medical Applications, Academic Press, San Diego, 1996.
[11] M. Anraku, Y. Tsurusaki, H. Watanabe, T. Maruyama, U. Kragh-Hansen, M. Otagiri, Stabilizing mechanisms in commercial albumin preparations: octanoate and N-acetyl-L-tryptophanate protect human serum albumin against heat and oxidative stress, Biochim. Biophys. Acta 1702 (2004) 9–17.
[12] Y. Ishima, T. Akaike, U. Kragh-Hansen, S. Hiroyama, T. Sawa, T. Maruyama, T. Kai, M. Otagiri, Effects of endogenous ligands on the biological role of human serum albumin in S-nitrosylation, Biochem. Biophys. Res. Commun. 364 (2007) 790–795.
[13] R.F. Chen, Removal of fatty acids from serum albumin by charcoal treatment, J. Biol. Chem. 242 (1967) 173–181.
[14] Y.A. Gryzunov, A. Arroyo, J.L. Vigne, Q. Zhao, V.A. Tyurin, C.A. Hubel, R.E. Gandley, Y.A. Vladimirov, R.N. Taylor, V.E. Kagan, Binding of fatty acids facilitates oxidation of cysteine-34 and converts copper-albumin complexes from antioxidants to prooxidants, Arch. Biochem. Biophys. 413 (2003) 53–66.
[15] T. Akaike, K. Inoue, T. Okamoto, H. Nishino, M. Otagiri, S. Fujii, H. Maeda, Nanomolar quantification and identification of various nitrosothiols by high performance liquid chromatography coupled with flow reactors of metals and Griess reagent, J. Biochem. (Tokyo) 122 (1997) 459–466.
[16] N. Ikebe, T. Akaike, Y. Miyamoto, K. Hayashida, J. Yoshitake, M. Ogawa, H. Maeda, Protective effect of S-nitrosylated alpha(1)-protease inhibitor on hepatic ischemia–reperfusion injury, J. Pharmacol. Exp. Ther. 295 (2000) 904–911.
[17] K. Inoue, T. Akaike, Y. Miyamoto, T. Okamoto, T. Sawa, M. Otagiri, S. Suzuki, T. Yoshimura, H. Maeda, Nitrosothiol formation catalyzed by ceruloplasmin. Implication for cytoprotective mechanism in vivo, J. Biol. Chem. 274 (1999) 27069–27075.
[18] M. Anraku, Y. Kouno, T. Kai, Y. Tsurusaki, K. Yamasaki, M. Otagiri, The role of N-acetyl-methioninate as a new stabilizer for albumin products, Int. J. Pharm. 329 (2007) 19–24.
[19] N.K. Holm, S.K. Jespersen, L.V. Thomassen, T.Y. Wolff, P. Sehgal, L.A. Thomsen, G. Christiansen, C.B. Andersen, A.D. Knudsen, D.E. Otzen, Aggregation and fibrillation of bovine serum albumin, Biochim. Biophys. Acta 1774 (2007) 1128–1138.
[20] Y. Ishima, T. Akaike, U. Kragh-Hansen, S. Hiroyama, T. Sawa, A. Suenaga, T. Maruyama, T. Kai, M. Otagiri, S-nitrosylated human serum albumin-mediated cytoprotective activity is enhanced by fatty acid binding, J. Biol. Chem. 283 (2008) 34966–34975.
[21] U. Kragh-Hansen, H. Watanabe, K. Nakajou, Y. Iwao, M. Otagiri, Chain length-dependent binding of fatty acid anions to human serum albumin studied by site-directed mutagenesis, J. Mol. Biol. 363 (2006) 702–712.

Journal of Controlled Release 145 (2010) 9–16

Contents lists available at ScienceDirect

Journal of Controlled Release

journal homepage: www.elsevier.com/locate/jconrel

Genetically engineered mannosylated-human serum albumin as a versatile carrier for liver-selective therapeutics

Kenshiro Hirata [a,1], Toru Maruyama [a,b,1], Hiroshi Watanabe [b], Hitoshi Maeda [a], Keisuke Nakajou [c], Yasunori Iwao [a], Yu Ishima [a], Hidemasa Katsumi [d,e], Mitsuru Hashida [d], Masaki Otagiri [a,f,*]

[a] Department of Biopharmaceutics, Graduate School of Pharmaceutical Sciences, Kumamoto University, 5-1 Oe-honmachi, Kumamoto 862-0973, Japan
[b] Center for Clinical Pharmaceutical Sciences, Kumamoto University, 5-1 Oe-honmachi, Kumamoto 862-0973, Japan
[c] The Pharmaceutical Research Center, Nipro Corporation 3023 Nojicho, Kusatsu, Shiga 525-0055, Japan
[d] Department of Drug Delivery Research, Graduate School of Pharmaceutical Sciences, Kyoto University, Sakyo-ku, Kyoto 606-8501, Japan
[e] Department of Biopharmaceutics, Kyoto Pharmaceutical University, Yamashina-ku, Kyoto 607-8414, Japan
[f] Faculty of Pharmaceutical Sciences, Sojo University, 4-22-1 Ikeda, Kumamoto 860-0822, Japan

ARTICLE INFO

Article history:
Received 23 October 2009
Accepted 13 March 2010
Available online 19 March 2010

Keywords:
Human serum albumin
Recombinant albumin
Mannosylation
Nitric oxide
Ischemia reperfusion

ABSTRACT

Human serum albumin (HSA), a non-glycosylated protein, is widely employed as carrier for drug delivery systems. A series of recombinant, mannosylated-HSA mutants (Man-rHSAs: D63N, A320T and D494N) and their triple mutant (TM-rHSA: D63N/A320T/D494N) were prepared, that can be selectively delivered to the liver *via* mannose receptor (MR) on the liver non-parenchymal cells. A pharmacokinetic analysis of ^{111}In-Man-rHSAs in mice showed that they were rapidly cleared from the blood circulation, and were largely taken up by the liver rapidly in the order: TM-rHSA > D494N ≫ A320T = D63N, consistent with their degree of mannosylation. *In vivo* competition experiments with an excess amount of chemically modified Man-BSA or mannan suggested that the hepatic uptake of TM-rHSA was selectively mediated by MR on Kupffer cells. Lastly, a TM-rHSA–NO conjugate, *S*-nitrosylated TM-rHSA, effectively delivered NO to the liver and then exhibited a significant inhibitory effect against hepatic ischemia/reperfusion injury model rats, accompanied by the induction of heme oxygenase-1.

1. Introduction

Human serum albumin (HSA) is the most abundant protein in plasma. The molecule is comprised of 585 amino acid residues with a MW of 66.7 kDa. HSA possesses multiple functions, including the maintenance of colloid osmotic pressure in plasma and the transport of various endogeneous substances and metabolite [1]. Because HSA has a simple molecular structure and is highly stable, it is frequently used to reduce immunogenicity associated with other therapeutics [1]. Thus, HSA is widely employed as a versatile carrier in drug delivery systems to improve pharmacokinetics and stability etc., thus improving the efficacy of therapeutics.

Since HSA does not contain canonical acceptor sequences (Asn-X-Thr/Ser tripeptide) required for *N*-glycosylation in its primary structure, it is not glycosylated in its native state. More than 60 genetic variants of HSA have been reported to date [2]. Researchers in several laboratories (including ours) have characterized the molecular, structural, biochemical and pharmacokinetic properties and stability of these genetic variants. Among them, three glycosylated HSA variants (albumin Darakallia, D63N; albumin Redhill, A320T; and albumin Casebrook, D494N) have been identified [3–5] because these mutant molecules contain the consensus sequence required for *N*-glycosylation. These variants behaved like wild-type HSA and possess similar properties. This leads to the conclusion that they might be potentially useful in therapeutic applications, especially as a carrier for a drug delivery system.

A number of suitable strategies for liver-selective targeting systems have been developed that involve the use of albumins that are chemically modified with substrates or ligands, such as sugars and peptides that bind receptors on the liver surface. One particularly interesting strategy involves the sugar recognition mechanism in which receptors recognize the corresponding sugars on the non-reducing terminal of sugar chains that are attached to albumin thereby mediating cellular uptake. Among these, chemically mannosylated (Man)-albumins have receive considerable attention because mannose receptors (MR), which specifically recognize ligands containing a terminal non-reducing D-mannose, N-acetylgluocosamine, or L-fucose, are expressed mainly on liver non-parenchymal cells, including Kupffer cells and sinusoidal endothelial cell [6,7]. Previous

Abbreviations: BSA, bovine serum albumin; CBB, Coomassie brilliant blue; DTPA, diethylenetriaminepentaacetic acid; DTT, dithiothreitol; Gal-BSA, galactosylated-BSA; GlcNAc, N-acetyl glucosamine; GSNO, *S*-nitroso glutathione; HO-1, heme oxygenase-1; HSA, human serum albumin; IR, ischemia reperfusion; man, mannose; man-BSA, mannosylated-BSA; Man-rHSAs, mannosylated-recombinant HSA mutants; PAS-stain, periodic acid Schiff-stain; ROS, reactive oxygen species; SNO-HSA, *S*-nitrosylated HSA; TM, triple mutant.

* Corresponding author. Tel.: +81 96 371 4150; fax: +81 96 362 7690.
E-mail address: otagiri@gpo.kumamoto-u.ac.jp (M. Otagiri).
[1] These authors contributed equally to this study.

0168-3659/$ – see front matter.
doi:10.1016/j.jconrel.2010.03.010

studies have clearly demonstrated that chemically modified Man-albumins are largely taken up by the liver *via* an MR-mediated mechanism. Despite such selective delivery, chemically modified Man-HSA has several limitations, for instance, its heterogeneity, an excess modification of lysine (Lys) residues etc. More recently, a recombinant albumin product purified from yeast has been made available on the market. When glycosylated proteins are expressed in a yeast system, they are highly mannosylated with oligosaccharides [8]. Therefore, if genetically engineered glycosylated recombinant HSA (rHSA) could be expressed by a yeast system, the resulting rHSA would contain high levels of the mannosylated form. These novel glycoproteins would be expected to be useful as a carrier for liver-selective therapeutics *via* MR. However, the production of rHSA that is genetically engineered to contain oligosaccharides and its therapeutic application has not been investigated.

Hepatic ischemia/reperfusion (IR) injury is a major clinical problem during perioperative periods and occurs frequently after major hepatic resection or liver transplantation. A growing body of evidence exists to suggest an impaired production of nitric oxide (NO) is a significant contributor to the pathogenesis of hepatic IR injury. As a result, a new strategy involving the delivery of NO to the liver has received much attention for the prevention of hepatic IR injury. *S*-nitrosylated proteins have several advantages over other NO donors. For example, they represent endogeneous NO reservoirs circulating in the blood [9], they induce minimal oxidative stress and high doses are not required to improve recovery from IR induced organ dysfunction [9]. In fact, we (and others) recently found that the administration of *S*-nitrosylated HSA (SNO-HSA) and derivatives thereof to animals with hepatic IR injury significantly reduce the extent of tissue damage [10], although the same concentrations of low molecular weight *S*-nitrosothiols produced no obvious protective effect on hepatic IR injury [11]. Therefore, it would appear that the targeted delivery of SNO-HSA to liver non-parenchymal cells would be a more effective approach to inhibiting liver injuries that are induced by IR.

The objective of this study was to develop novel, genetically engineered Man-rHSA mutants that have the potential to deliver therapeutics to the liver *via* MR localized on liver non-parenchymal cells. These molecules were prepared by inserting the consensus sequence for the *N*-glycoside binding motif using the above three genetically glycosylated variants as a template and a *Pichia pastoris* expression system, which resulted in the production of highly mannosylated forms of the protein. In this study, single mutants (D63N, A320T or D494N) and their triple mutant (TM: D63N/A320T/D494N) rHSAs were produced as candidates for use as liver-selective carriers and their physicochemical and pharmacokinetic properties were examined. Then, to address the potential of the molecules as carriers for liver-selective therapeutics, TM-rHSA-NO conjugate, *S*-nitrosylated TM-rHSA was prepared and its cytoprotective effect was examined using hepatic IR injury model rats.

2. Materials and methods

2.1. Materials and animal

Blue Sepharose 6 Fast Flow was obtained from GE Healthcare (Tokyo, Japan). Enzymes for DNA assays were obtained from Takara (Kyoto, Japan). The *Pichia* Expression kit was obtained from Invitrogen (Carlsbad, CA). Diethylenetriamine-pentaacetic acid (DTPA) was obtained from Dojindo Laboratories (Kumamoto, Japan). $^{111}InCl_3$ (74 MBq/ml in 0.02 N HCl) was a gift from Nihon Medi-Physics Co., Ltd. (Tokyo, Japan). Collagenase (type4) was obtained from Sigma Chemicals Inc. (St. Louis, MO, USA). All other chemicals were of the highest commercial grades available. Sprague–Dawley (SD) rats (180–210 g) were purchased from Kyudou Co. (Kumamoto, Japan). ddY mice were purchased from Japan SLC inc. (Saga, Japan). SD rats and ddY mice were maintained in a temperature-controlled room with a 12-hour dark/light cycle and free access to food and water. All animal experiments were performed according to the guidelines, principles, and procedures for the care and use of laboratory animals of Kumamoto University.

2.2. Generation of P. pastoris producing recombinant HSAs

The expression vector pPIC9-wild-type rHSA containing the wild-type rHSA expression cassette stably integrated into chromosomal DNA was used to produce rHSA [12]. The mutants were produced using a QuikChange XL site-directed mutagenesis kit (Stratagene, La Jolla, CA), with the following mutagenic primers (sense and antisense): 5′-GCTGAAAATTGTAACAAATCACTTCATACC-3′ and 3′-GGTATGAAGTGATTTGTTACAATTTTCAGC-5′ (D63N), 5′-GCAAAAAC-TATACTGAGGCAAAGG-3′ and 3′-CCTTTGCCTCAGTATAGTTTTTGC-5′ (A320T), 5′-GCTCTGGAAGTCAATGAAACATACG-3′ and 3′-CGTATGTTTCATTGACTTCCAGAGC-5′ (D494N). D63N/A320T/D494N was made by mutation of all mutation points. *P. pastoris* GS115 his4 was transformed with SalI-digested pPIC9-wild-type rHSA or pPIC9-mutant rHSAs by electroporation according to the manual (EasySelect *Pichia* Expression Kit Version A; Invitrogen). Histidine-independent transformants were selected and subsequently screened for slow methanol utilization phenotypes. Positive clones were induced by treatment with methanol and screened for the production of wild-type or mutant rHSAs by 10% SDS-PAGE of the culture medium.

2.3. Production and purification of recombinant HSAs

The protocol used to express the rHSA was a modification of a previously published protocol [12]. Single colonies of *P. pastoris* were grown (30 °C, 210 rpm, 48 h) in 300 ml of BMGY growth medium (1% yeast extract, 2% peptone, 100 mM potassium phosphate, pH 6.0, 1.34% yeast nitrogen base, 4×10^{-5}% biotin, and 1% glycerol) in 1-liter baffled flasks until an A_{600} value of 2 to 6 was obtained. Cells were then harvested by centrifugation at $3000\times g$, and the cell pellets were washed extensively and resuspended in 300 ml of BMMY medium (1% yeast extract, 2% peptone, 100 mM potassium phosphate, pH 6.0, 1.34% yeast nitrogen base, 4×10^{-5}% biotin, and 1% methanol) to an approximate A_{600} value of 15 to 20. For further culture of this *P. pastoris* suspension, the baffled flasks were shaken (30 °C, 190 rpm, 96 h) with the daily addition (every 12 h) of methanol at a final concentration of 1% to maintain the induction conditions of the alcohol oxidase 1 promoter. The recombinant proteins were purified after 96 h of induction, according to the literature [12]. The protein preparation was first subjected to chromatography with the Blue Sepharose 6 Fast Flow equilibrated with 50 mM sodium phosphate buffer (pH 7.0) after dialysis against the same buffer.

Proteins were further purified using a Phenyl HP column that had been equilibrated with 50 mM sodium phosphate buffer, pH 7.0, containing 0.65 M ammonium sulfate. The column was washed with phosphate buffer (50 mM, pH 7.0) and then eluted with 25 ml of ammonium sulfate in the same buffer (0.65 M). The eluted rHSAs were deionized and defatted by charcoal treatment, freeze-dried, and then stored at −20 °C until used. Sample purity was estimated by a density analysis of Coomassie brilliant blue (CBB)-stained protein bands on 10% SDS-PAGE. The recombinant protein samples of HSA and mutants were estimated to be more than 97% pure.

2.4. Synthesis of mannosylated HSA

Man-(12)-HSA was synthesized by reacting HSA with 2-imino-2-methoxyethyl 1-thioglycomannoside as previously described [13]. The product was dialyzed (molecular weight cutoff, 1000) against ultrapure water, and lyophilized. The number of sugar moieties was controlled by the amount of the sugar derivatives added to the reaction mixture and determined by the anthron method [14].

2.5. Synthesis of glycosylated bovine serum albumin (BSA)

Man-(42)-BSA and Gal-(55)-BSA were synthesized by reacting BSA with 2-imino-2-methoxyethyl 1-thioglycomannoside or thiogalactoside as previously described [13]. Each derivative was purified and concentrated by ultrafiltration (molecular weight cutoff, 10,000) against distilled water, and lyophilized. The number of sugar moieties was controlled by the amount of the sugar derivatives added to the reaction mixture and determined by the anthron method [14].

2.6. CBB-stain and periodic acid Schiff (PAS)-stain of SDS-PAGE

SDS-PAGE was performed using 10% polyacrylamide gel. The gel was stained with Coomassie brilliant blue R250 and Schiff's reagent solution for PAS.

2.7. Circular dichroism (CD) spectra measurement

CD spectra were obtained using JASCO J-720 spectroporalimeter (JASCO, Tokyo, Japan) at 25 °C. Far-UV and near-UV intrinsic spectra were recorded in the range from 200 to 250 nm and from 250 to 350 nm respectively. The protein concentration was determined to be 5 μM (far-UV) or 15 μM (near-UV) in PBS, respectively.

2.8. Pharmacokinetic analysis of recombinant HSAs and chemically modified Man-(12)-HSA

All proteins were radiolabeled with ^{111}In using the bifunctional chelating reagent DTPA anhydride according to the method of Hnatowich et al. [15]. Mice received tail vein injections of ^{111}In-labeled rHSAs and ^{111}In-labeled chemically modified Man-(12)-HSA in saline, at a dose of 0.1 mg/kg. In the early period after injection, the efflux of ^{111}In radioactivity from organs is assumed to be negligible, because the degradation products of ^{111}In-labeled ligands using DTPA anhydride cannot easily pass through biological membranes. This assumption was confirmed by the finding that no ^{111}In was detectable in the urine throughout the 120 min period. At appropriate intervals after the injection, blood was collected from the vena cava under ether anesthesia and plasma was obtained by centrifugation (3000×*g*, 10 min). The liver, kidney, spleen and lung were excised, rinsed with saline and weighed. The radioactivity of each sample was measured in a well-type NaI scintillation counter (ARC-500, Aloka, Tokyo). In the inhibition experiment using mannan, chemically modified Man-(42)-BSA or Gal-(55)-BSA, 50 times volume of mannan (5 mg/kg), 100 times excess of Man-(42)-BSA or Gal-(55)-BSA was simultaneously injected with ^{111}In-rHSAs. The radioactivity of all samples was related (percentages) to the total dose given to the animals.

2.9. Isolation of hepatic Kupffer cells and endothelial cells

The portal vein of rats were cannulated with a polyethylene catheter (diameter, 0.9 mm), and the liver perfused with 125 mL of Hank's balanced salt solution (HBSS) buffer (pH 7.5) without Ca^{2+} at a flow rate of 8 ml/min, then with 100 mL of HBSS buffer (pH 7.5) containing 0.05% collagenase and 4 mM $CaCl_2$ at 37 °C. The liver was minced and suspended in ice-cold HBSS containing 1% (w/v) BSA. The cell suspension was centrifuged 3 times at 50×*g* for 2 min. The supernatant was then centrifuged at 450×*g* for 10 min. The pellets were resuspended in 5 mL of DMEM and layered on top of a two-step Percoll gradient. The gradient consisted of 25% (v/v) Percoll (top) and 50% (v/v) Percoll (bottom). The gradient was centrifuged at 800×*g* for 30 min. Pure non-parenchymal cells banded at the interface between the two density cushions. Pure cultures of Kupffer cells were obtained by seeding purified non-parenchymal cells onto the surface of tissue culture plastic, followed by incubation for 20 min at 37 °C. Pure cultures of endothelial cells were obtained by transferring the nonadherent cells from these dishes to dishes coated with fibronectin, followed by incubation for 1 h at 37 °C. The purity of the isolated endothelial cells or Kupffer cells was assessed by phagocytosis (3 mm latex beads (obtained from Sigma-Aldrich Co. (St. Louis, MO)) or immunostaining (Anti-von Willebrand's Factor antibody produced in rabbit (obtained from Sigma-Aldrich Co. (St. Louis, MO)). The purity of both the isolated endothelial cells and Kupffer cells was over 98%.

2.10. Uptake of HSAs by Kupffer cells and endothelial cells

Endothelial cells isolated from a rat liver, as described above, were plated onto human fibronectin-coated 24-well plates (Becton Dickinson Lab., Bedford, U.K.) at 2×10^6 cells/well, and were grown in serum-free RPMI 1640 for 40 min at 37 °C. Each well was then washed 3 times with 0.75 ml of PBS to remove nonadherent cells, followed by incubation for 2 h with serum-free RPMI 1640. Kupffer cells were plated onto 24-well plates at 1×10^6 cells/well, and grown in Dulbecco's minimal essential medium (DMEM) for 20 min at 37 °C. Each well was then washed 3 times with 0.75 ml of PBS to remove nonadherent cells, followed by incubation for 24 h with DMEM. All cellular experiments were performed at 37 °C in a humidified atmosphere of 5% CO_2 in air. In the uptake experiments, the cells were washed twice with PBS and incubated at 37 °C with 0.5 ml of DMEM supplemented with 3% (w/v) BSA containing the indicated concentrations of ^{125}I-labeled rHSA with or without a 50-fold excess of unlabeled rHSA. The protein was radiolabeled with ^{125}I using the Iodo-gen (1,3,4,6-tetrachoro-3a,6a-diphenylglycoluri) method as previously described [16]. After incubation for 5 h, the culture medium was removed, and the remaining cells in each well were washed three times with 0.75 ml of PBS containing 1% (w/v) BSA, and twice more with PBS. The cells were lysed at 37 °C for 30 min with 0.5 ml of 0.1 M NaOH. One portion of the sample was used to measure the radioactivity of the cell-associated ligand, and the other portion was used to assay cellular proteins using a bicinchoninic acid protein assay (BCA) reagent (Pierce, Rockford, IL).

2.11. S-Nitrosylation of HSA

S-Nitrosylated protein was prepared under conditions that were protected from light and according to previously reported methods [10]. These samples were stored at −80 °C until used. The protein content of all protein preparations used in this study was determined by means of the Bradford assay.

2.12. Cytoprotective effect of SNO-HSAs and chemically modified Man-HSA in vivo

A rat IR liver injury model was employed to investigate the cytoprotective effect of SNO-HSAs and chemically modified Man-(12)-HSA, as previously reported [10]. Saline, as the vehicle control, or SNO-wild-type rHSA or SNO-TM-rHSA or SNO-Man-(12)-HSA (SNO-wild-type HSA, SNO-TM-rHSA and SNO-Man-(12)-HSA were injected at a dose of 0.035 μmol (*S*-nitroso content)/rat) was given *via* the portal vein immediately after the initiation of reperfusion. Plasma alanine aminotransferase (ALT) and aspartate aminotransferase (AST) activities levels were determined by using a transaminase C2 test kit from Wako Chemicals (Saitama, Japan), with activities expressed in international units per liter.

2.13. Western blot analysis

The portal vein of rats was cannulated with a polyethylene catheter (diameter, 0.9 mm), and the liver perfused with PBS. The liver was homogenized using BioMasher (Assist, Tokyo, Japan) with instructions. The resulting pellet is referred to as the liver homogenate. After measurement of the protein content using the BCA protein assay reagent (Pierce, Rockford, IL), each sample was mixed in a loading buffer (2% SDS, 333 mM Tris–HCl (pH 6.8), 10% glycerol,

100 mM DTT) and heated at 100 °C for 3 min. The sample were separated by 12.5% sodium dodecyl sulfate-polyacrylamide gel electrophoresis and transferred onto polyvinylidene difluoride membranes (Immobilon-P; Millipore, Bedford, MA) by semi-dry electroblotting. The blots were blocked for 1 h at room temperature with 5% ECL advance blocking agents (GE Healthcare Bio-sciences Corp., Piscataway, NJ) in PBS containing 0.05% Tween 20 (PBS-T). The blots were washed once with PBS-T and incubated for 1 h at room temperature with a primary antibody specific for heme oxigenase-1 (heme oxygenase-1 (C-20) affinity purified goat polyclonal antibody, Santa Cruz Biotechnology, Inc., Santa Cruz, CA) in PBS-T. The blots were washed 3 times with PBS-T and incubated with the secondary antibody (horseradish peroxidase-linked anti-goat IgG (H + L) (Invitrogen, Eugene, OR)) for 1 h at room temperature. The blots were washed 3 times with PBS-T and immunoblots were visualized using an ECL system (ECL Advance Western Blotting Detection Kit; GE Healthcare Bio-sciences Corp.) with LAS-4000EPUVmini (Fujifilm, Tokyo, Japan).

2.14. Measurement of liver NO_2^- and NO_3^- levels

NO_2^- and NO_3^- (NO_x) levels in liver homogenates were analyzed using an automated NO detector-high-performance liquid chromatographic system (ENO-10, Eicom, Kyoto, Japan) [17].

2.15. Data analyses

Pharmacokinetic analyses after rHSAs administration were based on a two-compartment model. Pharmacokinetic parameters were calculated by fitting using MULTI, a normal least-squares program [18]. The uptake clearance (CL_{uptake}) was calculated, as described in a previous report, using integration plot analysis at designated times (from 1 min to 30 min) during which the efflux and/or elimination of radioactivity from tissues were negligible [19]. Data are shown as means ± SD for the indicated number of animals. The overall differences between groups were determined by one-way of analysis of variance (ANOVA). A probability value of $p<0.05$ was considered to indicate statistical significance.

3. Results and discussions

3.1. Production of mannosylated recombinant HSAs (Man-rHSAs)

SDS-PAGE analysis clearly showed that the molecular weights of the mutants were increased slightly compared to that of wild-type rHSA, especially TM-rHSA, suggesting that multiple oligosaccharide chains were attached to TM-rHSA (Fig. 1A). To confirm that the increase in molecular weight of the mutants caused by newly introduced oligosaccharide chains, the periodic acid Schiff (PAS)-stain, which specifically stains oligosaccharide, was performed (Fig. 1B). In contrast to wild-type rHSA, all of the mutants reacted positively with the PAS-stain, indicating that the mutants clearly contained attached oligosaccharide chains.

The molecular weights of the rHSAs were determined to be 66537, 66849, 67097, 68977 and 69124 Da for wild-type, D63N, A320T D494N and TM-rHSA, respectively, by MALDI-TOF-MASS analyses. To deduce how many Man residues were attached to each mutant, we took into consideration 2 GluNAc (MW: 221 Da) in determining the numbers of Man residues because N-linked oligosaccharide chains expressed in *P. pastoris* generally consist of 2 GluNAc followed by 8 to 14 Man residues [20]. As a total number of residues, D63N, A320T, D494N and TM-rHSAs would be expected to contain 1–2, 2–3, 13 and 14 of GluNAc and Man residues, respectively. These findings are in good agreement with previous data reported on the characteristics of oligosaccharide chains in other recombinant glycoproteins expressed in *P. pastoris* [20].

3.2. Physicochemical properties of Man-rHSAs

To examine the effect of mutations as the result of the introduction of oligosaccharide chains on the secondary and tertiary structures of HSA, CD measurements were performed in the far- and near-UV regions (Fig. 2). All of the rHSAs showed nearly identical CD spectra in both UV regions, indicating that the mutations caused no significant effect on the secondary and ternary structure of HSA. In addition, the effect of mutations on surface charges of rHSA was estimated by capillary electrophoresis analysis. As expectedly, the retention times of the Man-rHSAs were not significantly different from that of wild-type rHSA (retention time: 9.1 min for wild type; 9.0 min for D63N;

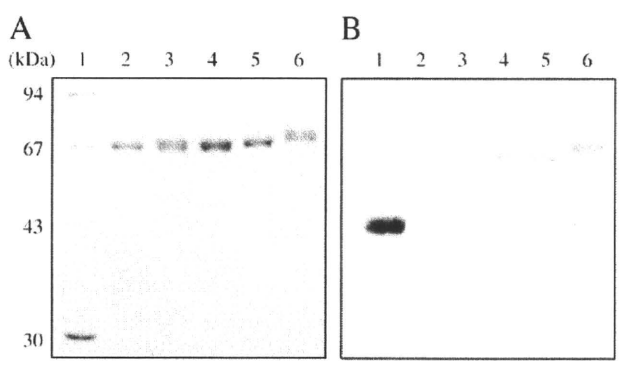

Fig. 1. SDS-PAGE analysis of rHSAs. A, CBB stained after SDS-PAGE. Lane 1, molecular weight marker; lane 2, wild type; lane 3, D63N; lane 4, A320T; lane 5, D494N; lane 6, TM. B, PAS stained after SDS-PAGE. Lane 1, α_1-acid glycoprotein; lane 2, wild type; lane 3, D63N; lane 4, A320T; lane 5, D494N; lane 6, TM.

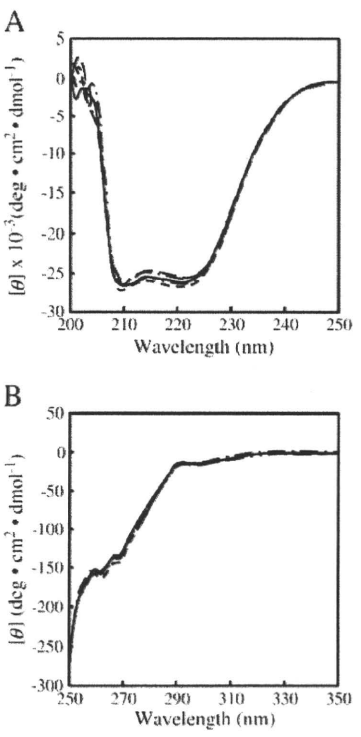

Fig. 2. CD spectra of rHSAs. A, far-UV and B, near-UV intrinsic spectra were recorded in the range from 200 to 250 nm and from 250 to 350 nm, respectively. The protein concentration was 5 μM (far-UV) or 15 μM (near-UV) in PBS at 25 °C, respectively. Spectra are shown for wild type (—), D63N (·····), A320T (------), D494N (-·-·-·) and TM (-··-··-).

9.0 min for A320T; 9.0 min for D494N; 8.9 min for TM). These data suggested that mutation and glycosylation neither affected the protein conformation nor the net charge of protein.

3.3. Pharmacokinetic properties and tissue distributions of Man-rHSAs

The fates of the ^{111}In-Man-rHSAs administered to mice were evaluated by determining the radioactivity in plasma. As shown in Fig. 3A, the pharmacokinetic profiles for D63N and A320T were similar to wild-type rHSA. In contrast, D494N and TM-rHSAs were rapidly cleared from the blood circulation compared to other rHSAs, including wild-type protein. Using these data, pharmacokinetic analysis was carried out and plasma clearance (CL_{tot}) were then estimated. CL_{tot} of wild type, D494N and TM-rHSAs were 0.8, 2.4 and 8.2 mL/h, respectively.

The tissue distributions of the Man-rHSAs were examined at 60 min after their administration. As shown in Fig. 3B, the tissue distribution patterns of the mutants, especially D494N and TM-rHSA were markedly changed compared to that of wild-type rHSA, which was largely present in the blood stream at 60 min. In the case of D494N and TM-rHSA, majority of the dose (50%, 65% for each mutant, respectively) after intravenous administration accumulated in the liver and small portions were also distributed to the kidney, lung and spleen.

Therefore, we further investigated the time course for the hepatic distribution of rHSAs (Fig. 3C). The hepatic uptake clearances (CL_{uptake} in liver) of D494N and TM-rHSA were 16 times and 47 times higher than that of wild-type rHSA (CL_{uptake} in liver; 0.13, 2.04 and 6.10 mL/h, for wild-type rHSA, D494N and TM-rHSA, respectively). These data clearly demonstrate that TM-rHSA was the most rapidly distributed and accumulated in the liver. Interestingly, the plasma clearances and liver distributions of Man-rHSAs were dependent on the degree of oligosaccharide modification, which was in the order of TM-rHSA > D494N ≫ A320T = D63N. These results indicate that the oligosaccharide chain attached to D494N plays an important role in the pharmacokinetic characteristics of TM-rHSA, while the other two positions contribute additionally. We have also compared the hepatic distribution of both ^{111}In-TM-rHSA and chemically modified ^{111}In-Man-(12)-HSA (parenthesis means the number of sugars). No significant differences between TM-rHSA and Man-(12)-HSA were observed in the hepatic distribution at 60 min after administration (65% for TM-rHSA; 66% for Man-(12)-HSA) and in the hepatic uptake clearance. These results suggested that hepatic distribution of TM-rHSA was similar to that of chemically modified Man-(12)-HSA.

To determine whether MR is involved in this rapid hepatic uptake pathway, we carried out an *in vivo* study in which the hepatic distribution of TM-rHSA was estimated in the presence of a100 times excess of chemically modified Man-(42)-BSA or 50 times excess of mannan, a well known substrate for MR. As shown in Fig. 3D, in the presence of Man-(42)-BSA or mannan, the hepatic distribution of TM-rHSA was decreased by about 90% or 50%, respectively, compared with that in the absence of these two MR substrates. On the other hand, no significant difference was observed in the presence of 100 times excess of chemically modified Gal-(55)-BSA, which is known to be taken up *via* asialoglycoprotein receptor expressed in liver parenchymal cells. Opanasopit et al. reported on *in vivo* inhibition experiments of ^{3}H-Man-liposomes with excess amounts of Man-BSA and Man-liposome [21]. They reported that Man-BSA and Man-liposome inhibited the uptake of ^{3}H-Man-liposomes by approximately 18% and 62%, respectively. In addition, the uptake of ^{125}I-Man-BSA was suppressed by nearly half by an excess amount of Man-BSA in *in vitro*

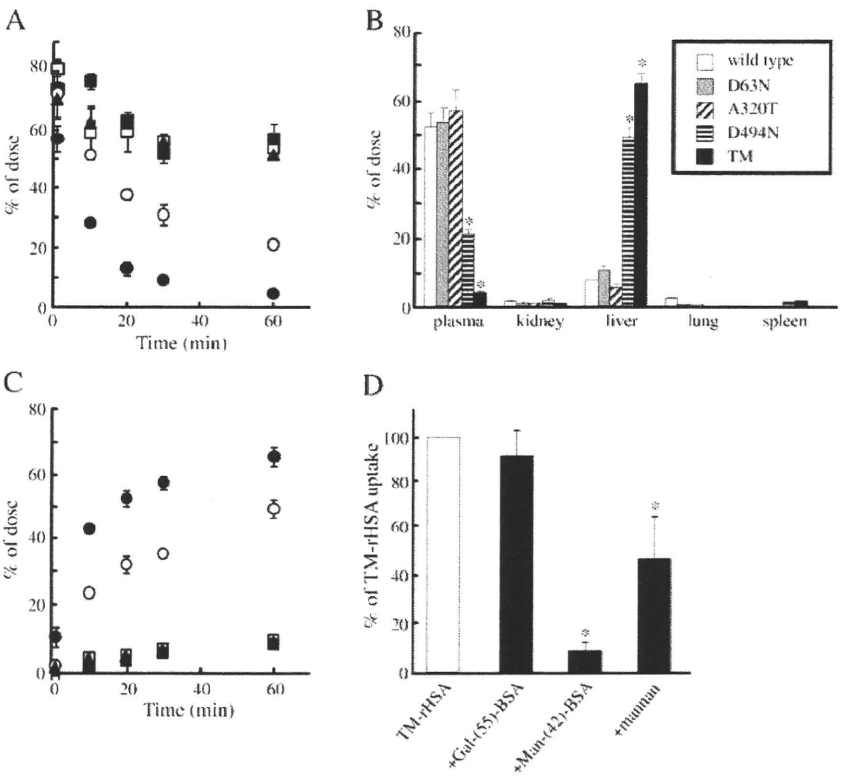

Fig. 3. A, Plasma concentration curve of rHSAs after 0.1 mg/kg of ^{111}In-rHSAs were injected in tail vein of mice. Filled triangle, filled square, open square, open circle and filled circle represent for wild type, D63N, A320T, D494N and TM, respectively. B, tissue distributions of rHSAs at 60 min. C, Hepatic uptake of rHSAs after ^{111}In-rHSAs were injected in tail vein of mice. Filled triangle, filled square, open square, open circle and filled circle represent for wild type, D63N, A320T, D494N and TM, respectively. Each value represents the mean ± SD. *$P<0.01$ as compared with wild-type. D, Effect of 100 times excess of Gal-(55)-BSA or Man-(42)-BSA and 50 times excess of mannan on hepatic distribution of TM. Each value represents the mean ± SD. *$P<0.01$ as compared with TM without inhibitor.

experiments using Kupffer cells [7]. In both studies, the investigators concluded that Man-liposome and Man-BSA were mainly taken up by the liver *via* MR. Thus, we conclude that MR plays pivotal role in the selective liver distribution of TM-rHSA. However, based on the present limited data, it is premature to conclude that other receptors such as scavenger receptors etc., are not involved in this process, and it must be necessary to examine the possibility of the contribution of other receptors.

3.4. Uptake of TM-rHSA by liver cells

To investigate which specific cells are responsible for the liver uptake of Man-rHSA, ^{111}In-labeled TM-rHSA was intravenously administrated to mice and the liver was then perfused with collagenase buffer, and separated into parenchymal cells and non-parenchymal cells. The findings indicate that more than 90% of the TM-rHSA is taken up by non-parenchymal cells (date not shown).

Furthermore, to examine which type of non-parenchymal cells are involved in the hepatic uptake of TM-rHSA, cellular uptake experiments were performed using primary-cultured endothelial cells and Kupffer cells. As a result, little uptake of ^{125}I-labeled TM-rHSA was observed in endothelial cells (Fig. 4A), while Kupffer cells took up TM-rHSA, specifically (Fig. 4B). This result suggests that MR on Kupffer cells are mainly involved in the specific uptake of TM-rHSA. Considering the physicochemical and pharmacokinetic analysis data, among the four Man-rHSAs, TM-rHSA was selected as a candidate for use as a liver-selective carrier and was only used following *in vitro* and *in vivo* experiments.

3.5. Cytoprotective effect of S-nitrosylated TM-rHSA after hepatic IR in rats

The over production of reactive oxygen species in Kupffer cells, the resident macrophages in the liver, during IR is one of the major causes of liver injury. Previous studies found that supplementation of NO to the liver stimulated the induction of heme oxygenase-1 (HO-1) expression, which has been shown to have anti-inflammatory actions and protect mammalian cells against various types of free radical damage [22]. Thus, the supplementation of NO to the liver including Kupffer cells has received considerable attention as a new and novel strategy for inhibiting liver damage, especially IR injury.

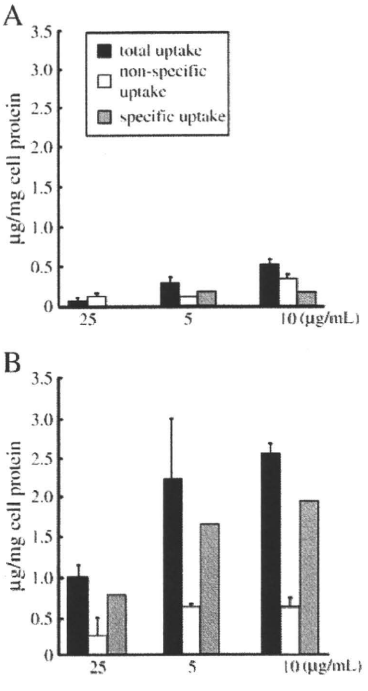

Fig. 4. Uptake of TM by liver non-parenchymal cells. A, Uptake of TM by endothelial cells and B, Uptake of TM by Kupffer cells. Specific uptake represents as total uptake minus nonspecific uptake. Total uptake and nonspecific uptake represents the mean ± SD.

To evaluate the potential of TM-rHSA as a NO traffic carrier to Kupffer cells, the effect of SNO-TM-rHSA on liver damage was examined using liver IR injury model rats. Since HSA contains only one free thiol group, i.e., Cys34, SNO-TM-rHSA was prepared by reacting TM-rHSA and isoamyl nitrite (described in the Materials and methods section). First, the *S*-nitroso content of TM-rHSA was estimated and found to be approximately 0.5 mol/mol protein which is higher than that of wild-type HSA (0.35 mol/mol protein). In a previous study, Ishima et al. reported that the administration of 0.01–0.1 μmol/rat of SNO-wild-type rHSA suppressed liver injury [10]. Thus, in this *in vivo* study, to compare the suppressive effects on liver damage, the *S*-nitroso content of both TM-rHSA and wild-type rHSA was adjusted to 0.035 μmol/rat and then injected into the liver injury model rats because the *S*-nitrosylation efficacies were different between two rHSAs, as discussed above.

The release of higher levels of liver enzymes AST and ALT was measured after the administration of SNO-TM-rHSA at the beginning of reperfusion. The effect of SNO-TM-rHSA was evaluated at 120 min after reperfusion, at which plasma AST and ALT levels were most increased [10]. As shown in Fig. 5A and B, SNO-wild-type rHSA effectively suppressed the IR injury. Interestingly, SNO-TM-rHSA inhibited IR injury more significantly than SNO-wild-type rHSA although an equivalent amount of NO was administrated. Wild-type and TM-rHSA (carrier alone) did not modify liver damage in this model (data not shown). These data suggest that SNO-TM-rHSA was more effective in delivering NO to Kupffer cells compared to SNO-wild-type HSA. To further compare the therapeutic efficacy with chemically modified Man-albumin, the effect of SNO-Man-(12)-HSA on hepatic IR injury was also examined in the same animal model. The results showed that the effect of SNO-Man-(12)-HSA after adjusting the *S*-nitroso content to 0.035 μmol/rat on hepatic IR injury was not significantly different from that of SNO-TM-HSA (data not shown), suggesting comparable efficacies between these two SNO-Man-albumins.

To confirm the effect of SNO-TM-rHSA, the total amount of NO derivatives, i.e., NO_2^- and NO_3^- were measured after SNO-TM-rHSA administration *in vivo* because NO is very reactive and is readily converted to derivatives. As shown in Fig. 5C, the total amount of NO_2^- and NO_3^- was significantly increased as the result of SNO-TM-rHSA treatment, while TM-rHSA itself had no effect on the total amount of derivatives. This indicates that NO is effectively delivered to the liver *via* MR by TM-rHSA. These data clearly support the proposed mechanism for enhanced cytoprotective activity of SNO-TM-rHSA, as outlined above. As mentioned in Introduction section, it has been believed that an impaired production of NO is a significant contributor to the pathogenesis of hepatic IR injury. However, in the present study, the measurement of NO_x concentrations in the liver did not demonstrate an impaired NO production upon IR treatment (saline-treated group with or without IR treatment). Such inconsistency might be due to the increase of the expression level of iNOS at 120 min post reperfusion, because generally, NO production is decreased in ischemia condition accompanied by a decrease in the eNOS activity and is increased in reperfusion condition accompanied by an increase in the iNOS expression. In fact, impaired production of NO in hepatic IR injury has been deduced by the changes of eNOS activity and there is no study on the measurement of NO_x levels in hepatocellular during reperfusion, so far. Thus, to clarify this, it will be necessary to evaluate the time course of the changes of NO_x level during the hepatic IR injury in future. In any case, the replacement of NO has potent cytoprotection against IR liver injury. In fact, it has been reported that genetic deficiency of the eNOS significantly exacerbates IR injury in

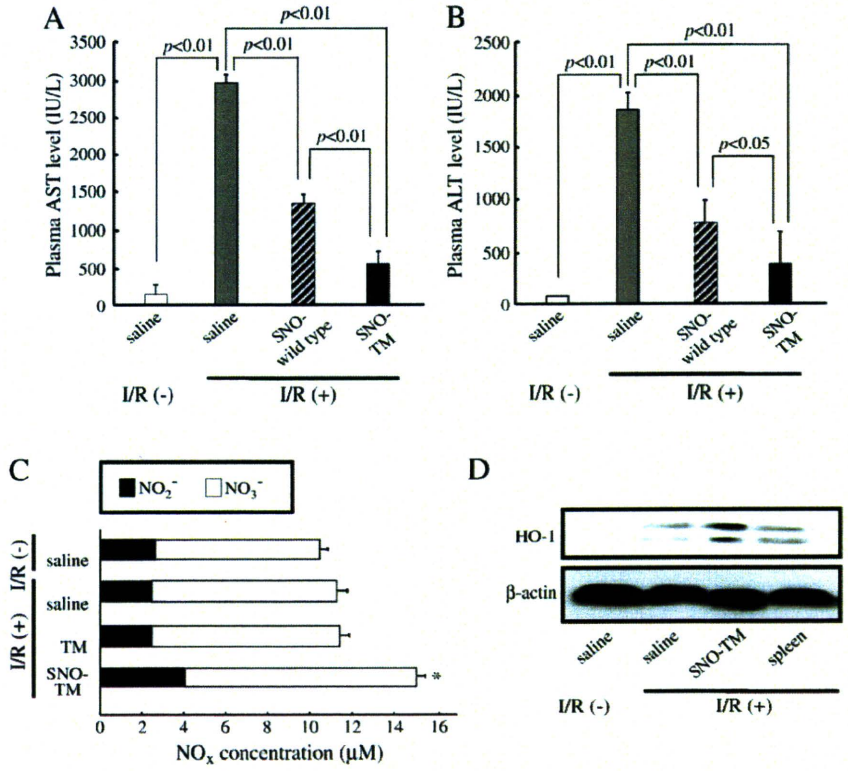

Fig. 5. Effect of SNO-TM on rat hepatic IR injury. SNO-wild type or SNO-TM was injected at beginning of reperfusion from the tail vain of rats after adjusting the *S*-nitroso content to 0.035 μmol/rat. A, plasma AST level at 120 min after reperfusion. B, plasma ALT level at 120 min after reperfusion. Each value represents the mean ± SD. *$P<0.01$ as compared with saline group with IR. C, NO_2^- and NO_3^- levels in liver. Liver was resected and homogenized at 120 min after reperfusion. Filled columns indicate liver NO_2^- levels and open columns indicate NO_3^- levels. Each value represents the mean ± SD. *$P<0.05$ as compared with saline group and TM group with IR (+). D, HO-1 induction by SNO-TM treatment on rat hepatic IR injury. HO-1 level was determined at 120 min after reperfusion. HO-1 level in spleen was also determined as a positive control.

heart whereas overexpression of eNOS attenuates IR injury [23]. This is further supported by the evidence that pharmacological inhibition of NOS exacerbates myocardial I/R injury [24], whereas administration of the NO precursor L-arginine can ameliorate myocardial I/R injury. In addition, Ishima et al. [10] and Ikebe et al. [11] have shown that S-nitrosylated albumin or *S*-nitrosylated α1-protease inhibitor treatment significantly ameliorate liver damage against IR injury in rats.

3.6. Effect of SNO-TM-rHSA on HO-1 protein expression in the liver

To investigate the mechanism of the cytoprotective activity of SNO-TM-rHSA, HO-1 level was determined by Western blotting analysis (Fig. 5D). As previously reported, IR treatment caused the induction of hepatic HO-1 [11]. Interestingly, the administration of SNO-TM-rHSA further significantly induced HO-1 in IR model rats. This is in good agreement with both the cytoprotective activity (Fig. 5A and B) and NO_2^- and NO_3^- levels (Fig. 5C), suggesting that these are interrelated. These findings lead to the proposed mechanism in which the cytoprotective effects of SNO-TM-rHSA could be due to the induction of hepatic HO-1 levels by delivered NO molecules. Devey et al. also demonstrated that Kupffer cell depletion resulted in the loss of HO-1 expression and increased susceptibility to hepatic IR injury [25]. Targeted deletion of HO-1 rendered mice highly susceptible to hepatic IR injury. Consequently, they concluded that there is a critical role for tissue-resident macrophages in homeostasis following ischemic injury, and a co-dependence of HO-1 expression and tissue-resident macrophage differentiation. Since NO strongly stimulates HO-1 expression [22], the approach proposed herein which deliver the NO to Kupffer cells seems to be effective in hepatic IR injury. This will be more clearly demonstrated by the comparable analysis using SNO-Gal-HSA or other glycosylated HSA. It is also suggested that the cytoprotective effects of *S*-nitrosothiol may involve multiple mechanisms, including 1) maintenance of tissue blood flow; 2) suppression of neutrophil infiltration; 3) reduction of apoptosis in the liver, in addition to 4) induction of HO-1, a cytoprotective enzyme [11].

3.7. Concluding remarks

In the present study, we successfully designed and genetically engineered TM-rHSA which has the ability to selectively deliver therapeutics to the liver *via* MR. To our knowledge, this is the first study to describe a genetically engineered rHSA with an oligosaccharide as a carrier for a drug delivery system and its therapeutic application. Our study showed that 1) among the four Man-rHSAs evaluated in this study, TM-rHSA was the most highly mannosylated and preserved the majority of the structural properties of wild-type HSA, 2) TM-rHSA was eliminated the most from the blood circulation and was then selectively taken up by the liver *via* MR on Kupffer cells, 3) SNO-TM-rHSA effectively delivered NO to the liver and exhibited a significant inhibitory effect against IR injury accompanied by the induction of HO-1. However, we have not explored the implication of the hepatic stellate cell, a non-parenchymal cell type in the liver that is known to have a crucial role when the liver is under hepatic fibrosis [26]. In addition, it was reported that an imbalance between endothelin and nitric oxide levels which results in the failure of hepatic microcirculation at the onset of reperfusion, and the activation of nuclear factor-kappa B in the liver which promotes proinflammatory cytokine and adhesion molecule synthesis contributed to the liver injury [27]. Therefore, examination of the effect of SNO-TM-rHSA on endothelin, inflammatory cytokine and adhesion molecule levels in addition to stellate cells activation should be one of the subjects of future investigation.

TM-rHSA was produced by inserting the consensus sequence for *N*-glycosylation using three genetically glycosylated HSA variants as a template and a *P. pastoris* expression system. Recombinant albumin products purified from yeast are currently coming on the commercial market. Basically, TM-rHSA can be produced by same bio-synthetic procedures using a recombinant albumin product. In addition, the results obtained here clearly demonstrated that this recombinant technique was able to be an alternative method for preparing Man-HSA without chemical modifications. Consequently, as compared to chemically modified Man-HSA, TM-rHSA can be prepared relatively homogeneous form and can be minimized the modification of reactive residues that attached the therapeutics and surface charges of HSA, which is favorable for producing a stable preparation. Furthermore, in the present study, only NO was tested as a therapeutic compound. However, this delivery system is not only limited to NO but has widespread applications for other liver therapeutics, such as drugs, cytokines, proteins, hormones etc. Therefore, TM-rHSA would be expected to become versatile carrier for liver-selective therapeutics.

Acknowledgements

We acknowledge Ms. Tamami Kimura for their technical assistance. This research was supported [in part] by Grant-in-Aid for Scientific Research from Japan Society for the Promotion of Science (JSPS) (KAKENHI 18390051 and 21390177).

References

[1] V.T. Chuang, U. Kragh-Hansen, M. Otagiri, Pharmaceutical strategies utilizing recombinant human serum albumin, Pharm. Res. 19 (2002) 569–577.
[2] L. Minchiotti, M. Campagnoli, A. Rossi, M.E. Cosulich, M. Monti, P. Pucci, U. Kragh-Hansen, B. Granel, P. Disdier, P.J. Weiller, M. Galliano, A nucleotide insertion and frameshift cause albumin Kenitra, an extended and O-glycosylated mutant of human serum albumin with two additional disulfide bridges, Eur. J. Biochem. 268 (2001) 344–352.
[3] S.O. Brennan, T. Myles, R.J. Peach, D. Donaldson, P.M. George, Albumin Redhill (-1 Arg, 320 Ala--Thr): a glycoprotein variant of human serum albumin whose precursor has an aberrant signal peptidase cleavage site, Proc. Natl Acad. Sci. USA 87 (1990) 26–30.
[4] J. Carlson, Y. Sakamoto, C.B. Laurell, J. Madison, S. Watkins, F.W. Putnam, Alloalbuminemia in Sweden: structural study and phenotypic distribution of nine albumin variants, Proc. Natl Acad. Sci. USA 89 (1992) 8225–8229.
[5] R.J. Peach, S.O. Brennan, Structural characterization of a glycoprotein variant of human serum albumin: albumin Casebrook (494 Asp--Asn), Biochim. Biophys. Acta 1097 (1991) 49–54.
[6] T.R. Gemmill, R.B. Trimble, Overview of N- and O-linked oligosaccharide structures found in various yeast species, Biochim. Biophys. Acta 1426 (1999) 227–237.
[7] Y. Higuchi, M. Nishikawa, S. Kawakami, F. Yamashita, M. Hashida, Uptake characteristics of mannosylated and fucosylated bovine serum albumin in primary cultured rat sinusoidal endothelial cells and Kupffer cells, Int. J. Pharm. 287 (2004) 147–154.
[8] Y. Yabe, M. Nishikawa, A. Tamada, Y. Takakura, M. Hashida, Targeted delivery and improved therapeutic potential of catalase by chemical modification: combination with superoxide dismutase derivatives, J. Pharmacol. Exp. Ther. 289 (1999) 1176–1184.
[9] Y.R. Kuo, F.S. Wang, S.F. Jeng, B.S. Lutz, H.C. Huang, K.D. Yang, Nitrosoglutathione promotes flap survival via suppression of reperfusion injury-induced superoxide and inducible nitric oxide synthase induction, J. Trauma 57 (2004) 1025–1031.
[10] Y. Ishima, T. Sawa, U. Kragh-Hansen, Y. Miyamoto, S. Matsushita, T. Akaike, M. Otagiri, S-Nitrosylation of human variant albumin Liprizzi (R410C) confers potent antibacterial and cytoprotective properties, J. Pharmacol. Exp. Ther. 320 (2007) 969–977.
[11] N. Ikebe, T. Akaike, Y. Miyamoto, K. Hayashida, J. Yoshitake, M. Ogawa, H. Maeda, Protective effect of S-nitrosylated alpha(1)-protease inhibitor on hepatic ischemia–reperfusion injury, J. Pharmacol. Exp. Ther. 295 (2000) 904–911.
[12] S. Matsushita, Y. Isima, V.T. Chuang, H. Watanabe, S. Tanase, T. Maruyama, M. Otagiri, Functional analysis of recombinant human serum albumin domains for pharmaceutical applications, Pharm. Res. 21 (2004) 1924–1932.
[13] Y. Yabe, N. Kobayashi, M. Nishikawa, K. Mihara, F. Yamashita, Y. Takakura, M. Hashida, Pharmacokinetics and preventive effects of targeted catalase derivatives on hydrogen peroxide-induced injury in perfused rat liver, Pharm. Res. 19 (12) (2002) 1815–1821.
[14] T.A. Scott, E.H. Melvin, The determination of dextran with anthrone, Anal. Chem. 25 (1953) 1656–1661.
[15] D.J. Hnatowich, W.W. Layne, R.L. Childs, The preparation and labeling of DTPA-coupled albumin, Int. J. Appl. Radiat. Isot. 33 (5) (1982) 327–332.
[16] S. Matsushita, V.T. Chuang, M. Kanazawa, S. Tanase, K. Kawai, T. Maruyama, A. Suenaga, M. Otagiri, Recombinant human serum albumin dimer has high blood circulation activity and low vascular permeability in comparison with native human serum albumin, Pharm. Res. 23 (5) (2006) 882–891.
[17] M. Tabuchi, K. Umegaki, T. Ito, M. Suzuki, I. Tomita, M. Ikeda, T. Tomita, Fluctuation of serum NO(x) concentration at stroke onset in a rat spontaneous stroke model (M-SHRSP). Peroxynitrite formation in brain lesions, Brain Res. 949 (2002) 147–156.
[18] K. Yamaoka, Y. Tanigawara, T. Nakagawa, T. Uno, A pharmacokinetic analysis program (multi) for microcomputer, J. Pharmacobiodyn. 4 (11) (1981) 879–885.
[19] M. Murata, I. Tamai, Y. Sai, O. Nagata, H. Kato, Y. Sugiyama, A. Tsuji, Hepatobiliary transport kinetics of HSR-903, a new quinolone antibacterial agent, Drug Metab. Dispos. 26 (11) (1998) 1113–1119.
[20] V. Blanchard, R.A. Gadkari, G.J. Gerwig, B.R. Leeflang, R.R. Dighe, J.P. Kamerling, Characterization of the N-linked oligosaccharides from human chorionic gonadotropin expressed in the methylotrophic yeast Pichia pastoris, Glycoconj. J. 24 (2007) 33–47.
[21] P. Opanasopit, M. Sakai, M. Nishikawa, S. Kawakami, F. Yamashita, M. Hashida, Inhibition of liver metastasis by targeting of immunomodulators using mannosylated liposome carriers, J. Control. Release 80 (2002) 283–294.
[22] C. Bouton, B. Demple, Nitric oxide-inducible expression of heme oxygenase-1 in human cells. Translation-independent stabilization of the mRNA and evidence for direct action of nitric oxide, J. Biol. Chem. 275 (42) (2000) 32688–32693.
[23] S.P. Jones, J.J. Greer, A.K. Kakkar, P.D. Ware, R.H. Turnage, M. Hicks, R. van Haperen, R. de Crom, S. Kawashima, M. Yokoyama, D.J. Lefer, Endothelial nitric oxide synthase overexpression attenuates myocardial reperfusion injury, Am. J. Physiol. Heart Circ. Physiol. 286 (1) (2004) H276–H282.
[24] R. Pabla, A.J. Buda, D.M. Flynn, D.B. Salzberg, D.J. Lefer, Intracoronary nitric oxide improves postischemic coronary blood flow and myocardial contractile function, Am. J. Physiol. 269 (3Pt 2) (1995) H1113–H1121.
[25] L. Devey, D. Ferenbach, E. Mohr, K. Sangster, C.O. Bellamy, J. Hughes, S.J. Wigmore, Tissue-resident macrophages protect the liver from ischemia reperfusion injury via a heme oxygenase-1-dependent mechanism, Mol. Ther. 17 (1) (2009) 65–72.
[26] E. Broide, E. Klinowski, G. Koukoulis, N. Hadzic, B. Portmann, A. Baker, E. Scapa, G. Mieli-Vergani, Superoxide dismutase activity in children with chronic liver diseases, J. Hepatol. 32 (2) (2000) 188–192.
[27] F. Serracino-Inglott, N.A. Habib, R.T. Mathie, Hepatic ischemia–reperfusion injury, Am. J. Surg. 181 (2) (2001) 160–166.

Drug Metabolism Reviews, 2011, 1–12, Early Online

ISSN 0360-2532 print/ISSN 1097-9883 online
DOI: 10.3109/03602532.2011.558094

informa
healthcare

REVIEW ARTICLE

Pharmacokinetic properties of hemoglobin vesicles as a substitute for red blood cells

Kazuaki Taguchi[1], Toru Maruyama[1,2], and Masaki Otagiri[1,3]

[1]Department of Biopharmaceutics, Kumamoto University, Kumamoto, Japan, [2]Center for Clinical Pharmaceutical Sciences, Graduate School of Pharmaceutical Sciences, Kumamoto University, Kumamoto, Japan, and [3]Faculty of Pharmaceutical Sciences, Sojo University, Kumamoto, Japan

Abstract

The development of artificial oxygen carriers has attracted considerable recent interest because of the increasing cost of collecting and processing blood, public concerns about the safety of blood products, complications from blood transfusions, military requirements for increased volumes of blood during military conflicts, and a decrease in the number of new donors. To overcome these problems, perfluorocarbon-based oxygen carriers as well as acellular- and cellular-type, hemoglobin-based oxygen carriers have been developed for use as artificial oxygen carriers. Despite their extensive evaluation, including formulation and pharmacology, they have not been extensively used in clinical settings. One of the reasons for this is that their pharmacokinetics have not been well characterized. Artificial oxygen carriers require not only an acceptable level of physicochemical activity, but also clinical efficacy, as reflected by their retention in the circulation, and the absence of measurable accumulation in the body, if unexpected adverse effects are to be avoided. In this review, the pharmacokinetic properties of artificial oxygen carriers are discussed, with a focus on recent developments of our research related to the pharmacokinetic properties a cellular type of hemoglobin-based oxygen carrier.

Keywords: Artificial oxygen carrier, disposition, liposome, mononuclear phagocyte system, hemorrhagic shock, hepatic chronic cirrhosis, accelerated blood clearance phenomenon

Introduction

In modern medical care, there is now little doubt that the transfusion of red blood cells (RBCs) is the gold standard for treatment of patients with massive hemorrhages and is currently in widespread use. Nevertheless, the potential for mismatching exists and infections by unrecognized pathogens, hepatitis, HIV, or West Nile virus, etc., are always a possibility. In addition, ensuring a steady supply of RBCs at a time of a disaster and during military conflicts could be difficult, because the lifetime of donated RBCs is limited to a short period. Further, a decrease in donors and an increase in recipients in some developed countries is also a problem. To overcome these problems, various artificial oxygen carriers have been under development worldwide. They can be divided into three major classes of materials, as follows: perfluorocarbon-based oxygen carriers, acellular-type, hemoglobin-based oxygen carriers (HBOCs), and cellular-type HBOCs (Figure 1). Despite the many efforts to develop artificial oxygen carriers during the past several decades, some of them were, unfortunately, rejected for use as the result of preclinical and clinical trials. It is noteworthy that perfluorocarbon-based oxygen carriers and acellular-type HBOCs were excluded as possible candidates for artificial oxygen carriers, even though they proceeded to the stage of clinical trials.

One of the reasons that induced these adverse effects was due to the insufficient characterization of pharmacokinetics of these artificial oxygen carriers under various situations. The desirable features of artificial oxygen carriers as a substitute for RBCs is not only a long retention in the circulation to sustain its pharmacological effects, but also no bioaccumulation, which could lead to adverse effects. Unlike other drugs, because the dosage volume of

Address for Correspondence: Masaki Otagiri, Department of Biopharmaceutics, Graduate School of Pharmaceutical Sciences, Kumamoto University, 5-1 Oe-honmachi, Kumamoto 862-0973, Japan; Fax: +81-96-362-7690; E-mail: otagirim@gpo.kumamoto-u.ac.jp

(Received 05 October 2010; revised 22 January 2011; accepted 24 January 2011)

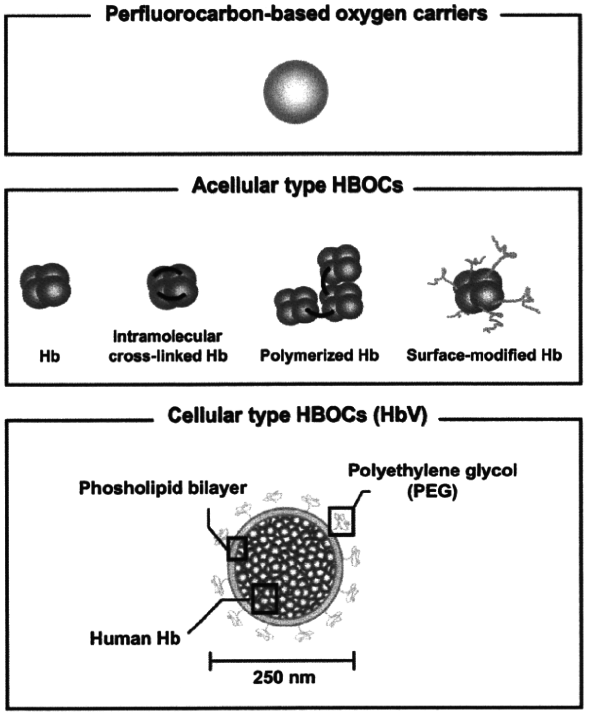

Figure 1. Schematic representation of perfluorocarbon-based oxygen carriers, acellular-type hemoglobin-based oxygen carriers (HBOCs), and cellular-type HBOCs (HbV). In the case of HbV, the surface is modified with polyethylene glycol (PEG) chains, and one HbV particle contains approximately 30,000 human Hb molecules obtained from outdated donated blood. The encapsulated Hb contains pyridoxal 5'-phosphate as an allosteric effector to regulate P_{50} to 25–28 torr. The lipid bilayer was comprised of a mixture of DPPC, cholesterol, and DHSG at a molar ratio of 5:5:1, and DSPE-PEG_{5000} (0.3 mol%). The average particle diameter was regulated to approximately 250 nm.

an artificial oxygen carrier as an RBC substitute is more than a hundred times higher than that of other drugs, detailed information regarding the fate of an artificial oxygen carrier, including its constituent components, is needed, in order to predict unexpected adverse effects.

In this review, the pharmacokinetic properties of artificial oxygen carriers are discussed, with a focus on hemoglobin vesicles (HbVs), in which, among the current artificial oxygen carriers, its pharmacokinetic properties have been extensively characterized.

Perfluorocarbon-based oxygen carriers

The perfluorocarbon-based oxygen carriers are characterized by a high gas-dissolving capacity, low viscosity, and chemical and biological inertness (Spahn and Kocian, 2003). They are molecules that are constructed from cyclic or straight-chain hydrocarbons, in which the hydrogen atoms are replaced by halogens, and are virtually immiscible with water and, therefore, must be emulsified prior to their use in intravenous applications (Pape and Habler, 2007). When perfluorocarbon emulsion droplets are injected into an organism, they are rapidly taken up and slowly broken down by the mononuclear phagocyte system (MPS). After being degraded, the emulsion droplets are again taken up by the blood and transported to the lungs, where any unaltered molecules are excreted via exhalation (Spahn and Kocian, 2003; Jahr et al., 2007; Pape and Habler, 2007). However, perfluorocarbon-based oxygen carriers induced chronic pneumonitis due to their inefficient excretion from the body and their accumulation in the lung, a condition that persists for more than 1 year (Nose, 2004) (Table 1).

Acellular-type HBOCs

The stroma-free hemoglobin (Hb) was developed for use as artificial oxygen carriers, but their systemic half-lives were too short (~0.5–1.5 hours) for them to effectively function as an optimal oxygen carrier (Savitsky et al., 1978). In addition, the Hb tetramers dissociate into their component αβ dimers, which are then eliminated by the kidneys, and induce renal toxicity (Creteur and Vincent, 2003). In an attempt to increase their systemic half-life and stability, the following three groups of chemically modified acellular-type HBOCs were developed: surface-modified Hb (Smani, 2008), intramolecularly cross-linked Hb (Chen et al., 2009), and polymerized Hb (Jahr et al., 2008) (Figure 1). These acellular HBOCs have improved systemic half-lives, in the range of 18–24 hours, and show decreased renal failure (Stowell, 2005) (Table 1). The polymerized bovine-derived Hb has been approved for limited use in South Africa (Lok, 2001). However, it was recently reported that the use of some acellular-type HBOCs leads to the development of myocardial lesions, as the result of decreasing nitric-oxide levels 24–48 hours after a single topload infusion (Burhop et al., 2004), leading to an increase in mortality rates in humans (Natanson et al., 2008).

Hemoglobin vesicles

The hemoglobin vesicle (HbV) is a cellular-type HBOC that contains polyethylene glycol (PEG), in which phospholipid vesicles encapsulating highly concentrated human Hb are imbedded (Sakai et al., 2008) (Figure 1). The cellular structure of HbV (particle diameter: approximately 250 nm) most closely mimics the characteristics of a natural RBC, such as the cell-membrane function, which physically prevents the direct contact of Hb with the components of blood and the vasculature during its circulation. The characteristics of HbV are superior to donated RBCs in the following ways: the absence of viral contamination (Sakai et al., 1993; Abe et al., 2001), a long-term storage period of over 2 years at room temperature, and no blood-type antigens (Sakai et al., 2000; Sou et al., 2000) (Table 2). In addition, HbVs have the ability to transport oxygen equivalent to RBCs and also show improved survival in hemorrhagic shock animal models (Sakai et al., 2004b; Terajima et al., 2006; Sakai et al., 2009). Further, HbVs can control the release of oxygen by

adjusting the amount of allosteric effector and regulate rheological properties (e.g., viscosity and colloid osmotic pressure) to added human serum albumin (Sakai and Tsuchida, 2007). Therefore, HbV has attracted considerable attention as a possible new artificial oxygen carrier and has considerable promise for use in clinical settings.

We recently characterized the pharmacokinetic properties of HbV to clarify its efficacy and safety under conditions that mimic a clinical setting, as follows:

1. HbV was constructed from multiple components, including Hb, lipids, and iron from Hb. These components have potential risks for inducing harmful effects, when they accumulate at excessive levels in the body.
2. HbV is classified as a liposome preparation. It was previously reported that the pharmacokinetics of liposome-encapsulated amphotericin B differ between normal individuals and patients (Walsh et al., 1998; Bekersky et al., 2001).
3. The surface of HbV was modified by PEG to enhance the half-life in circulation and storage. It was recently reported that repeated injection of PEGylated liposomes influenced the pharmacokinetics of the second injected liposome (Dams et al., 2000; Ishida et al., 2003a).

Table 1. Pharmacokinetic properties of some artificial oxygen carriers.

	Perfluorocarbon-based oxygen carriers	Acellular-type HBOCs	Cellular-type HBOCs
Distribution	Liver, spleen	Liver	Liver, spleen
Metabolism	MPS	MPS	MPS
Excretion	Air	—	Internal Hb; urine outer membrane; feces
Half-life	~10 hours (rat)	~24 hours (rat)	30~40 hours (rat)
Existence in tissues	~1 year	—	~14 days

HBOCs, hemoglobin-based oxygen carriers; MPS, mononuclear phagocyte system.

Table 2. Physicochemical characteristics of HbV.

Parameter	
Particle diameter	ca. 250 nm
P_{50}	25–28 torr
Hb concentration	10 g/dL
MetHb	<3%
Colloid osmotic pressure	0 Torr
Intracellular Hb concentration	ca. 35 g/dL
Lipid composition[a]	DPPC/cholesterol/DHSG/DSPE-PEG_{5000}
Stability for storage at room temperature	Over 2 years, purged with N_2

[a]DPPC, 1,2-dipalmitoyl-*sn*-glycero-3-phosphatidylcholine; DHSG, 1,5-bis-*O*-hexadecyl-*N*-succinyl-L-glutamate; DSPE-PEG_{5000}, 1,2-distearoyl-*sn*-glycero-3-phosphatidyl-ethanolamine-*N*-PEG.

For these reasons, it becomes necessary to clarify the pharmacokinetic properties of HbV in various animal models and under conditions of repeated injection, if RBCs are to be used as a substitute in the future. For this purpose, 1) the disposition of HbVs was examined using isotope tracer techniques. In these experiments, ^{125}I-HbV, enclosed in HbVs, was radiolabeled with ^{125}I, and the lipid component vesicles of HbVs was radiolabeled with ^{3}H; 2) a pharmacokinetic study of HbVs in a rat model of hemorrhagic shock and hepatic chronic cirrhosis; 3) the repeated injection in normal and the hemorrhagic shock rat model; and 4) animal scale-up using an allometric equation, were conducted.

Some highlights of recent developments of our research related to the pharmacokinetic properties of HbV are discussed below.

The prior pharmacokinetic characteristics of HbV to stroma-free Hb

Two requirements need to be satisfied if HbV is to be accepted for use as an artificial oxygen carrier. For clinical applications, HbVs must have not only an acceptable physicochemical activity, but also must be safe for use in the clinic. In the latter case, the supply of oxygen tissues is one of the most important factors in sustaining the clinical effect of HbVs (Takaori, 2005). To fulfill these requirements, a prolonged half-life is a required property for HbVs.

We recently demonstrated that the half-life of HbV in mice was 30 times higher than that of stroma-free Hb at a dose rate of 1 mg Hb/kg (Table 3). Moreover, a dose-dependent study clearly showed that the plasma concentration curve and half-life of HbV in mice and rats increased with increasing doses of HbV (Figure 2, half-life; rats: 8.8±0.7, 11.5±0.3, and 30.6±4.0 hours at doses of 10, 200, and 1,400 mg Hb/kg, respectively; mice: 3.1±3.1, 3.6±1.3, 7.2±3.1, and 18.8±1.3 hours at doses of 1, 10, 200, and 1,400 mg Hb/kg, respectively) (Taguchi et al., 2009b).

These superior pharmacokinetic characteristic of HbV, compared to stroma-free Hb, could reflect their physicochemical differences, such as particle diameter, the absence or presence of a membrane structure, and PEG modification. In physiological conditions, free Hb that is released from ruptured RBC is rapidly bound to

Table 3. Pharmacokinetic parameters for HbV after the administration of ^{125}I-Hb and ^{125}I-HbV in mice at a dose of 1 mg Hb/kg.

	^{125}I-Hb	^{125}I-HbV	*p*
$t_{1/2}$ (hr)	0.1±0.1	3.1±1.0	<0.01
AUC (hr*% of dose/mL)	7.9±3.9	29.4±9.2	<0.001
CL (mL/hr)	12.7±2.1	3.4±0.1	<0.001
V (mL)	2.6±0.3	2.3±0.1	N.S.

$t_{1/2}$, half-life; AUC, are under the plasma-concentration versus time curve; CL, clearance; V, distributed volume; N.S., not significant.

haptoglobin (Hp), which promotes CD163 recognition in the liver (Kristiansen et al., 2001). When the Hb concentration exceeds the Hp-binding capacity, unbound Hb is removed by filtration through the kidney. Therefore, the reduction in HbV distribution in the liver and kidney could be due to the encapsulation of Hb by liposomes because this might not only suppress the binding of internal Hb to Hp, but also inhibit renal glomerular filtration. In fact, it was observed that the distribution of HbV in the liver and kidney was suppressed, compared with that of stroma-free Hb (Taguchi et al., 2009b). Moreover, the membrane surface modification by PEG also contributed to the increased half-life of HbV. In general, it is well-known that liposomes are scavenged and degraded by the MPS, such as Kupffer cells or macrophages in the spleen (Kiwada et al., 1998). PEGylation is a useful method for suppressing the capture of MPS, and the majority of the recently developed liposome formulations are modified with PEG (Noble et al., 2006; Sou et al., 2007; Okamura et al., 2009). Therefore, the modification of HbV with PEGylation is important to not only stabilize for a long-time storage, but also to maintain the good retention in the circulation. These balanced physicochemical activities result in a longer retention in the circulation, compared to stroma-free Hb and acellular-type HBOCs (Goins et al., 1995; Chang et al., 2003; Lee et al., 2006).

The disposition of HbV components

In clinical situations as a substitute of RBCs, massive amounts of HbV are typically given to patients. As a result, its associated components, including Hb, lipids from Hb, could result in undesirable consequences in the systemic circulation and organs during its metabolism and disposition. Such an extraordinary load of HbV components could result in the accumulation of components in the blood or organs, and has the potential to cause a variety of adverse effects, as follows: 1) high levels of lipid components, especially cholesterol, in the bloodstream, which are risk factors for kidney disease, arterial sclerosis, and hyperlipidemia (Grone and Grone, 2008); 2) Hb induces renal toxicity by dissociation of the tetramic Hb subunits into two dimers (Parry, 1988); and 3) free iron can trigger tissue damage induced by the Fenton reaction, which is mediated by heme (iron) (Balla et al., 2005). Therefore, it becomes necessary to clarify whether HbV and its components have favorable metabolic and excretion profiles. In order to investigate the disposition of each HbV component, Hb, enclosed in HbV, was radiolabeled with ^{125}I (^{125}I-HbV) or cholesterol, in the lipid component vesicles of HbV, was radiolabeled with ^{3}H (^{3}H-HbV).

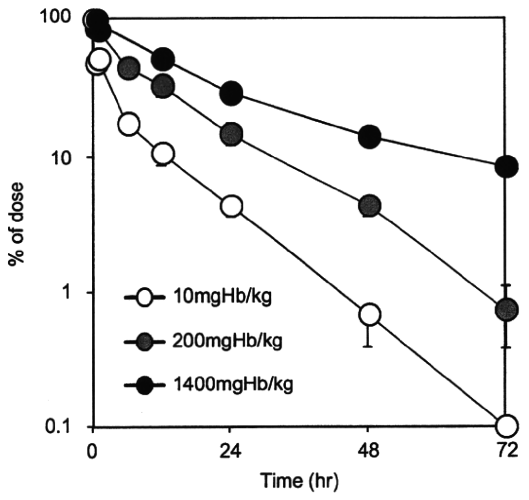

Figure 2. Dose-dependent plasma concentration curve of ^{125}I-HbV after administration of ^{125}I-HbV in rats. All rats received a single injection of ^{125}I-HbV at a dose of 10 (open squares), 200 (gray circles), and 1,400 mg Hb/kg (closed circles) containing 5% rHSA. At each time point (0.05, 0.5, 1, 6, 12, 24, 48, and 72 hours) after the ^{125}I-HbV injection, blood samples were collected from the tail vein, and a plasma sample was obtained. Each point represents the mean ± SD (n=3–5).

In the blood circulation, HbV typically maintains an intact structure for periods of up to 72 hours after injection, because similar plasma concentration curves for ^{125}I-HbV were observed for ^{3}H-HbV in rats (Figure 3A), and the pharmacokinetic parameters were also consistent between them (half-life: 30.6 ± 4.0, 30.9 ± 4.7 hours; clearance in plasma: 0.46 ± 0.04, 0.41 ± 0.02 mL/h, for ^{125}I- and ^{3}H-HbV, respectively). Moreover, ^{125}I-HbV and ^{3}H-HbV were mainly distributed in the liver and spleen (Figure 3B). Because HbV possesses a liposome structure, it would be predicted that it would be captured by the MPS in the liver and spleen (Kiwada et al., 1998). In fact, a previous *in vitro* study clearly demonstrated that HbV was specifically taken up and degraded in RAW 264.7 cells, which has been used as an alternative to Kupffer cells, but this was not the case for parenchymal and endothelial cells (Taguchi et al., 2009b). In addition, the uptake clearance (CL_{uptake}) in the liver and spleen were also similar between the two labeled preparations (liver: 1,141 ± 142, 1,098 ± 123; spleen: 619 ± 40, 518 ± 89 μL/h, for ^{125}I-HbV and ^{3}H-HbV, respectively). However, ^{125}I was more rapidly eliminated from each organ, and the activity essentially disappeared within 7 days. On the other hand, the elimination of radioactive ^{3}H was delayed, compared to that of ^{125}I, but nearly disappeared after 14 days. These data indicate that HbV is mainly distributed to the liver and spleen in the form of intact HbV, and that it was degraded by the MPS. In order to identify the excretion pathway of HbV, the levels of radioactivity of ^{125}I and ^{3}H in the urine and feces were measured. The radioactive ^{125}I was excreted mainly in the urine, whereas the majority of the ^{3}H was excreted in the feces. Based on the above findings, the disposition of HbV and its components, after circulating in the form of stable HbV, are distributed to the liver and spleen, where they are degraded by the MPS. Finally, the enclosed Hb and outer lipid components were mainly eliminated to the urine and feces, respectively, in the same manner as endogeneous substances (Figure 4). Similar results were also reported in mice and rabbits (Sou et al.,

2005; Taguchi et al., 2009b); these results indicate that HbV and its components have favorable metabolic and excretion profiles in mammalian species. In addition, the plasma concentration curve for heme (iron) derived from HbV was similar to that for ^{125}I-HbV and ^{3}H-HbV in mice (Taguchi et al., 2009b). Moreover, no significant differences in the ratio of the mercapt- (i.e., nonoxidized form) to the nonmercapt-form (i.e., oxidized form) of rat serum albumin, which serves as a marker of oxidative stress in the circulation system (Kadowaki et al., 2007; Shimoishi et al., 2007), were found between HbV and the saline administration groups for periods of up to 7 days after administration. These results suggest that excess free heme (iron) derived from HbV is not released in the plasma. However, the issue of the disposition of several HbV components, including PEG and phospholipid, was not clarified. It is also possible that these components in HbV are also metabolized and excreted in the same manner as endogenous substances, but further study will be needed to demonstrate this fact.

Pharmacokinetic properties of HbV under conditions of hemorrhagic shock

It is well known that clinical conditions can have an effect on the pharmacokinetics of numerous drugs (Abernethy et al., 1981; Turck et al., 1996). For example, it has demonstrated that the pharmacokinetics of liposome-encapsulated amphotericin B differ between normal individuals and patients in a clinical trial stage (Walsh et al., 1998; Bekersky et al., 2001). Consequently, it is possible that the pharmacokinetics of HbV would be also altered in the situation of a massive hemorrhage caused by injury, accidental blood loss, or a major surgery. To clarify this, we investigated the changes in HbV pharmacokinetics using a rat model of hemorrhagic shock induced by massive hemorrhage.

As shown in Figure 5, the retention of HbV in plasma under this condition was shorter, and the half-life of HbV was reduced significantly—by 0.66-fold—compared with the half-life of HbV in normal rats (30.6 ± 4.0, 18.1 ± 3.7 hours, for normal and hemorrhagic shock, respectively). At a glance, this appears to not be a desirable situation for the therapeutic use of HbV, because an important determinant of HbV efficacy is a long retention in the blood circulation. However, the distribution volume of the central compartment of HbV (V_1) was identical between normal and hemorrhagic shock rats, whereas the distribution volume of the peripheral compartment (V_2) in hemorrhagic shock rats was nearly 2-fold greater than that of normal rats (Figure 5, insert). Moreover, the time-course tissue distribution of HbV in the hemorrhagic shock rats was greater than normal rats. These findings indicate that the shorter half-life in hemorrhagic shock rats appears to be the result in an apparent reduction in HbV in the arteriovenous circulation. If this enhanced tissue distribution of HbV might be derived by an increased scavenging of HbV by the MPS, such as by Kupffer cells, red pulp zone splenocytes, and mesangial cells (Sakai et al., 2004a), it would not be expected to show significant pharmacological efficacy as an oxygen carrier, because HbV must maintain an intact structure to maintain its oxygen-carrying capacity. However, the pharmacological effect in the hemorrhagic shock model animal was significantly increased by the HbV treatment, similar to that for an RBC treatment (Sakai et al., 2004b; Terajima et al., 2006; Sakai et al., 2009). In addition, the amount of excretion into the urine, which is the major elimination pathway, did not differ between normal and hemorrhagic shock rats in our pharmacokinetic study. Therefore, HbV appears to be transferred from the arteriovenous blood to organ capillary beds as an intact structure, and is not excessively captured and metabolized by the MPS. These findings support the conclusion

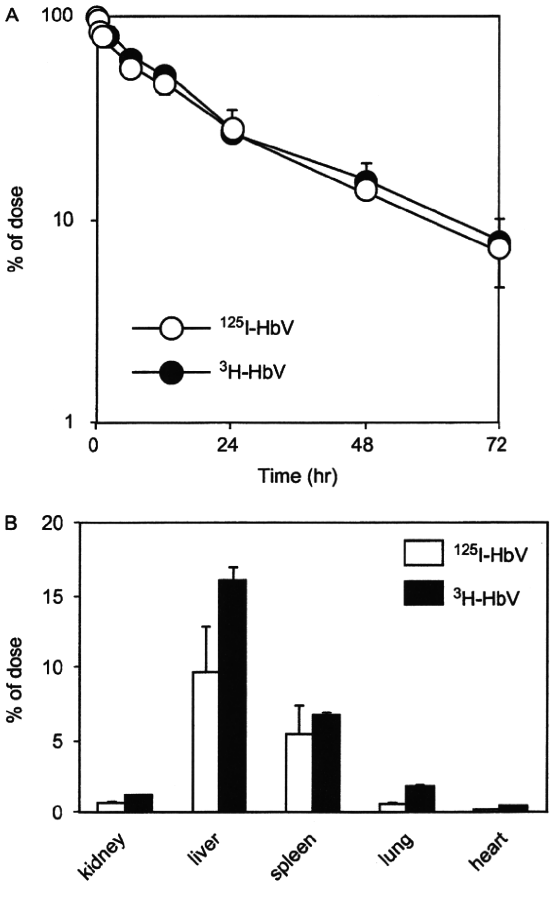

Figure 3. (**A**) Time course for the plasma level of ^{125}I-HbV (open circles) and ^{3}H-HbV (filled circles) after administration to rats. SD rats received a single injection of ^{125}I-HbV or ^{3}H-HbV to the tail vain at a dose of 1,400 mg Hb /kg. Blood was collected from the tail vein under ether anesthesia, and a plasma sample was obtained. Each point represents the mean ± SD (n=5). (**B**) Tissue distributions of ^{125}I-HbV (open bars) and ^{3}H-HbV (filled bars) at 24 hours after administration to mice. SD rats received a single injection of ^{125}I-HbV or ^{3}H-HbV from the tail vain at a dose of 1,400 mg Hb/kg. At 24 hours after injection, each organ was collected. Each bar represents the mean ± SD (n=5).

that HbV is pharmacologically efficacious in a rat model of HS induced by massive hemorrhage (Sakai et al., 2004b, 2009) is retained for a sufficiently long period to meet oxygen-delivery demands until autologous blood volume and oxygen-carrying capacity are restored.

Pharmacokinetic properties of HbV in the condition with chronic liver failure

As mentioned above, the liver is the determinant for the pharmacokinetic properties of HbV, because HbV is mainly degraded by Kupffer cells, and the lipid components of HbV, especially cholesterol, are excreted to the feces via biliary excretion (Sakai et al., 2001; Taguchi et al., 2009b). Consequently, HbV can be classified as a hepatically cleared and excreted drug. In the case of other hepatically cleared and excreted drugs, some are contraindicated for a person with a hepatic injury. Because hepatic impairment affects the pharmacokinetics of drugs, including their metabolism and excretion (Okumura et al., 2007), these changes have the potential to induce toxicity and accumulate in the body, subsequently causing unexpected adverse effects. Thus, if HbV and its components show the changes of pharmacokinetic properties under conditions of liver failure, it may also be contraindicated for a person with liver impairment under such conditions. Therefore, we investigated the pharmacokinetic properties of HbV using a chronic cirrhosis rat model with fibrosis induced by the administration of carbon tetracholoride, which is categorized as Child-Pugh grade B (Taguchi et al., 2011b).

After the administration of HbV to chronic cirrhosis rats, the plasma concentration of HbV varied widely among individuals, similar to their liver function. To clarify the effect of hepatic impairment on the plasma concentration of HbV, the clearance and the area under the concentration-time curve values for HbV, as calculated from the plasma concentration curve, were plotted against plasma aspartate aminotransferase (AST) levels. As a result, a good, negative correlation was found for the clearance of HbV with changes in plasma AST levels. In addition, the hepatic distribution of HbV was negatively

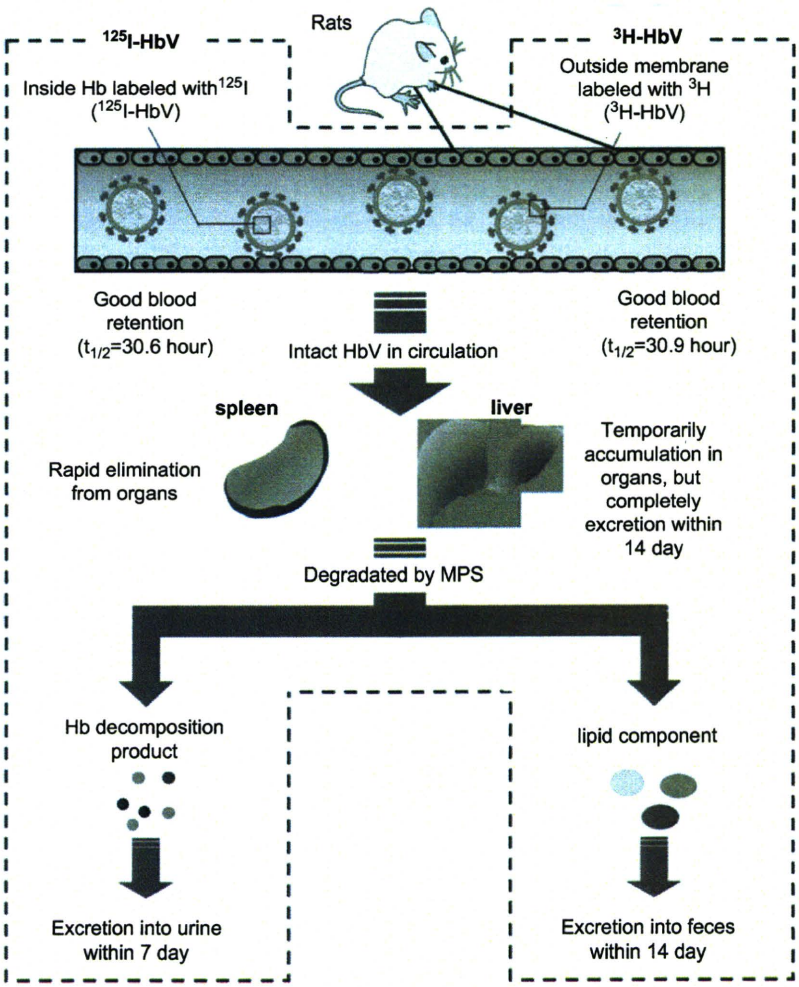

Figure 4. Representation of a sequence of HbV disposition, metabolism, and excretion from pharmacokinetic examinations, using ^{125}I-HbV and ^{3}H-HbV. After circulating in the form of stable HbV, it is distributed to the liver and spleen, where it is degraded by MPS. Finally, the enclosed Hb and outer lipid components are mainly eliminated to the urine and feces, respectively.

correlated with plasma AST levels, but this was not found for the spleen. Moreover, carbon clearance, which serves as a measure of phagocyte activity in Kupffer cells (Zweifach and Benacerraf, 1958), was also negatively correlated with plasma AST levels. Therefore, the changes in HbV pharmacokinetic properties were significantly influenced by a reduction in liver function and were especially dependent on a decrease in phagocyte activity by Kupffer cells in the chronic cirrhosis rat.

In addition, the excretion of lipid components (e.g., cholesterol) in feces was also negatively correlated with plasma AST levels. The cholesterol of the vesicles should reappear in the blood mainly as lipoprotein cholesterol after entrapment by Kupffer cells and should then be excreted in the bile after entrapment of the lipoprotein cholesterol by the hepatocytes (Kuipers et al., 1986). Therefore, the extent of damage to parenchymal cells also affects the pharmacokinetic properties of HbV components. Such a suppressed elimination of HbV components may have an impact on their tissue accumulation. However, the lipid components, especially cholesterol, nearly completely disappeared from organs after 7 days in the chronic cirrhosis rat. Further, our recent study showed that the plasma levels of other lipid components, such as phospholipids, was temporarily increased after the administration of HbV at a dose of 1,400 mg Hb/kg in the chronic cirrhosis rat, but recovered to baseline levels within 14 days (Taguchi et al., 2010). In addition, if the metabolic and excretion performance of HbV were reduced by chronic cirrhosis, tissue damage could be induced, resulting in a change in blood biochemical parameters. However, the morpholgical changes in organs were minimal (Figure 6), and only negligible changes in plasma biochemical parameters were observed after an HbV injection at a dose of 1,400 mg Hb/kg in the chronic cirrhosis rats. Based on these findings, it can be concluded that the pharmacokinetics of HbV were altered by hepatic impairment, and these changes can be attributed to a decrease in Kupffer-cell phagocyte activity (Figure 7). However, HbV and its components were completely metabolized and excreted within 14 days, and a temporary accumulation did not cause any obvious adverse effects.

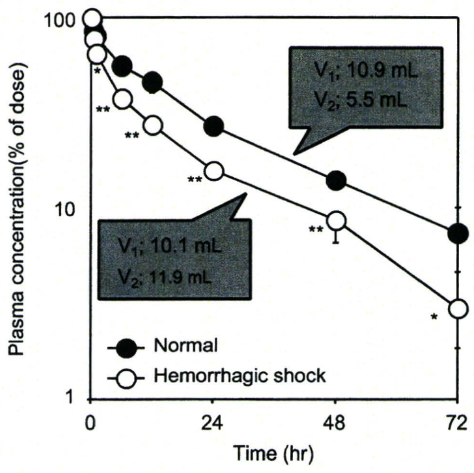

Figure 5. Relative plasma concentration of ^{125}I-HbV after administration of 1,400 mg Hb/kg via injection of normal (filled circles) or hemorrhagic shock rats (open circles). After inserting polyethylene catheters into the left femoral artery, SD rats received a single injection of ^{125}I-HbV to the left femoral artery at a dose of 1,400 mg Hb /kg. Blood was collected from the tail vein under ether anesthesia, and a plasma sample was obtained. Each point represents the mean ± SD (n=5).

Pharmacokinetic properties of HbV after repeated administration in mice

HbV is modified by PEG to prolong its half-life and prevent aggregation during long-term storage, etc., as well

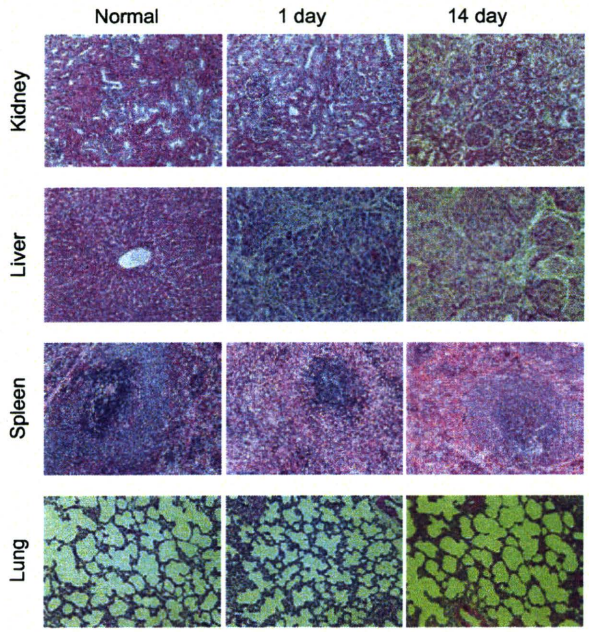

Figure 6. Light micrographs of kidney, liver, spleen, lung, and heart in CCl_4-treated rats after an HbV injection stained with hematoxylin and eosin (X100). Chronic cirrhosis model rats received a single injection of HbV at a dose of 1,400 mg Hb/kg. No noticeable changes were observed in all organs after HbV injection.

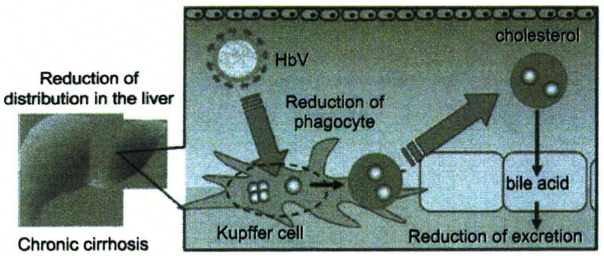

Figure 7. Representation of the pharmacokinetic properties of HbV in a rat model of chronic cirrhosis. Hepatic impairment altered the pharmacokinetic properties of HbV, such as blood retention, hepatic distribution, and fecal excretion, by a reduction in Kupffer cell phagocyte activity and damage to parenchymal cells.

as other liposome preparations. However, it was reported that repeated intravenous injection of PEGylated liposomes causes the second dose of liposomes to lose their long-circulating characteristics and accumulate extensively in the liver, when they are administrated at the same dose for the second time to the same animal within a several-day interval [referred to as the accelerated blood clearance (ABC) phenomenon] (Dams et al., 2000; Ishida et al., 2003a). The time frame between administration of the first and second dose for this to occur depends on the experimental animal, for example, 4–5□days for the rat and 7–10 days for the mouse. Repeated HbV injections of high doses would be routinely used in clinical practice for an RBC substitute. Therefore, the possibility remains that repeated injections of HbV could induce the ABC phenomenon in a clinical situation. If the ABC phenomenon were induced by repeated injections, then the pharmacological action of HbV could be influenced. Therefore, we investigated the issue of whether HbV induces the ABC phenomenon in mice at a low dose (0.1 mg Hb/kg), a dose that is generally known to induce the ABC phenomenon (Ishida et al., 2003a), or a high dose (1,400 mg Hb/kg), the putative dose for clinical use.

At 7 days, in which the ABC phenomenon in mice is typically observed the most strongly (Ishida et al., 2003b), after the first injection of nonlabeled HbV (0.1 or 1,400 mg Hb/kg), the mice received ^{125}I-HbV. At a low dose (0.1 mg Hb/kg), plasma HbV in the second injection was rapidly cleared, compared to that in the first injection. In contrast, at a high dose (1,400 mg Hb/kg), the pharmacokinetics of HbV were negligibly affected by repeated injections (Taguchi et al., 2009c). The liver and spleen are the major distribution organs for HbV (Taguchi et al., 2009b) and are related to the induction of

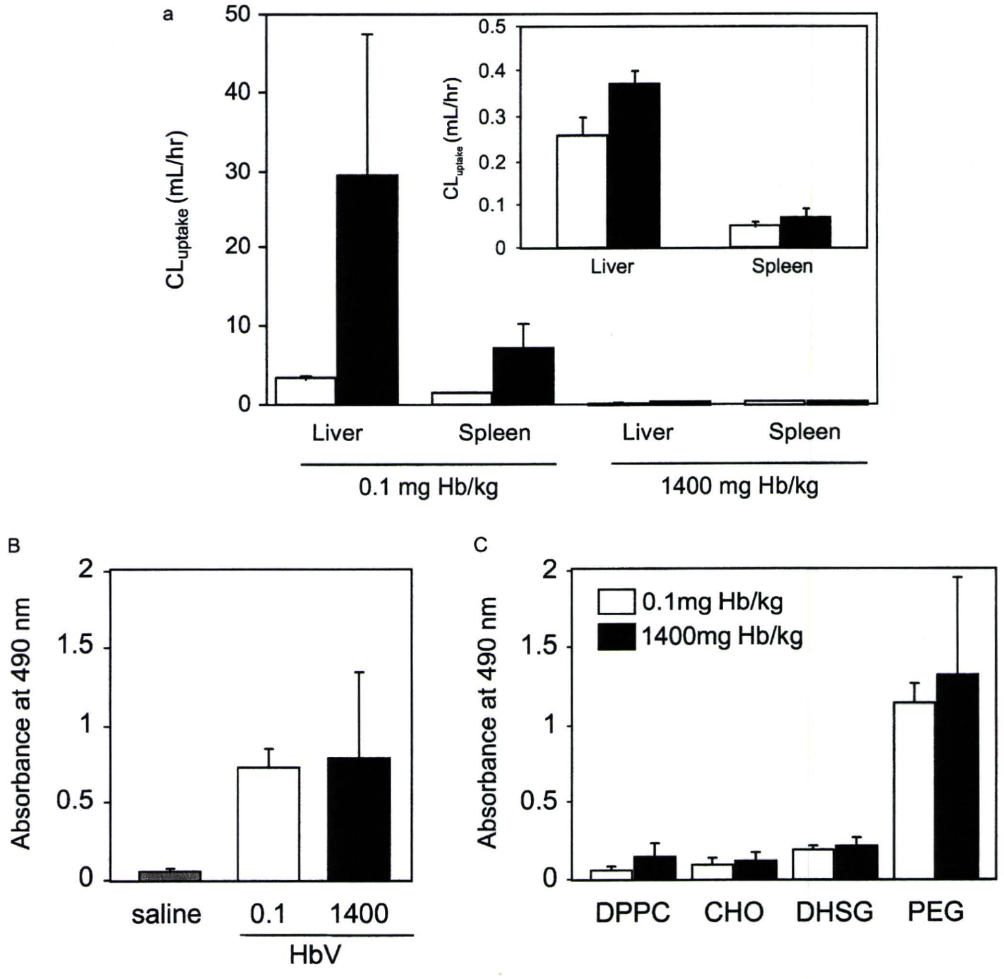

Figure 8. (**A**) Uptake clearance of HbV in the liver and spleen after 1 or 2 injections of ^{125}I-HbV. Uptake clearance for each organ was calculated by integration plot analysis at designated times from 1 to 30 minutes after injection. Each bar represents the mean ± SD (n=4). (**B**) Determination of IgM against HbV after a single intravenous injection of saline (gray bars), HbV at a dose of 0.1 mg Hb/kg (open bars), or 1,400 mg Hb/kg (closed bars) in mice. (C) Determination of the specific recognition site of IgM against HbV after a single intravenous injection of HbV at a dose of 0.1 mg Hb/kg (open bars) or 1,400 mg Hb/kg (closed bars) in mice. DdY mice were injected with saline or HbV (0.1 or 1,400 mg Hb/kg) containing 5% rHSA to the tail vein. At 7 days after an injection of saline or HbV, blood was collected from the inferior vena cava, and plasma was obtained. IgM against HbV and each lipid component were detected by ELISA. Each bar represents the mean ± SD (n=4).

the ABC phenomenon (Ishida et al., 2008). At a low dose, the hepatic and splenic CL_{uptake} for the second injection was 8.5 and 4.5 times higher than that for the first injection, respectively (Figure 8A), whereas at a high dose, the hepatic and splenic CL_{uptake} for the second injection was little changed, compared to that for the first injection (Figure 8A, insert). In addition, Ishida et al. proposed a mechanism for the ABC phenomenon as follows: Immunoglobulin M (IgM), produced in the spleen by the first injection with PEGylated liposomes, selectively binds to the PEG on the second injected PEGylated liposome, and subsequent complement activation by IgM results in an accelerated clearance and enhanced hepatic uptake of the second injected PEGylated liposome (Ishida et al., 2006a, 2006b). Therefore, we examined whether IgM against HbV is elicited by an initial injection of saline or HbV at a low or high dose. At 7 days after the HbV injection, IgM against HbV appeared at both the low and the high dose (Figure 8B). Moreover, the specific recognition site of IgM against HbV strongly bound to DSPE-PEG, and other lipid components (DPPC, cholesterol, and DHSG) were negligible at both the low and high dose (Figure 8C). These results indicate that repeated injections of HbV to mice at a dose of 1,400 mg Hb/kg did not appear to induce the ABC phenomenon, even though the plasma levels of IgM against HbV are elevated. Therefore, these data suggest that a clinical dose of HbV is not likely to induce the ABC phenomenon due to the saturation of phagocytic processing by the MPS.

Pharmacokinetic properties of HbV after repeated administration in hemorrhagic shock model rats

Because there are limited data available for the ABC phenomenon under various disease conditions, we also investigated whether the ABC phenomenon would be induced in the rat model of hemorrhagic shock induced by a massive hemorrhage, when HbV is injected at a dose of 1,400 mg Hb/kg at hourly intervals, typical conditions for transfusions of patients with massive hemorrhage.

The plasma concentration of HbV was prolonged in the second injection, compared with the first injection, and it was recovered to that in normal rats (Figure 9A). As mentioned above, Ishida et al. reported that a dosing interval of approximately 5 days induced the ABC phenomenon in rats, accompanied by the production of antiliposome IgM, which elicits a response by the spleen (Ishida et al., 2006b; Wang et al., 2007). Therefore, the inhibition of anti-HbV IgM production by short intervals appears to prevent induction of the ABC phenomenon. In fact, anti-HbV IgM was detected at 5 days after the administration of HbV to normal rats at a dose of 0.1 mg Hb/kg, but was not detected at 1 hour after HbV administration to hemorrhagic shock rats at a dose of 1,400 mg Hb/kg (Figure 9B). Therefore, it appears that the repeated administration of HbV under conditions of hemorrhagic shock has negligible effect on the pharmacokinetics of HbV, when short dosing intervals are involved. However, our recent study showed that the repeated injection of HbV induced the ABC phenomenon in the case of a longer dosing interval (4 and 7 days) accompanied by the production of antiliposome IgM and increased phagocyte activity (Taguchi et al., 2011a). Therefore, in a clinical setting, it would be necessary to consider the dosing regimen and interval for patients with hemorrhagic shock in the base where a longer dosing interval was used.

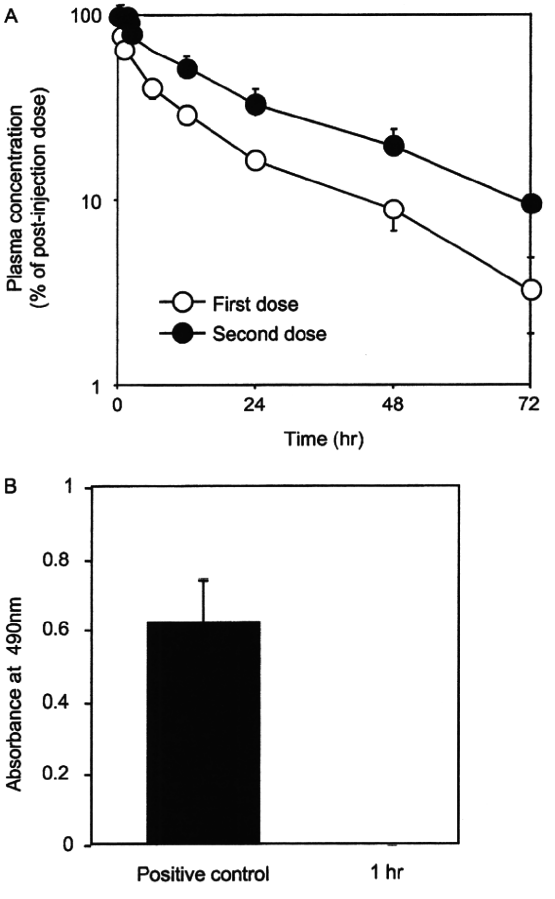

Figure 9. (A), Plasma concentration of ^{125}I-HbV as the percent of postinjection dose after the first (open symbol) or second dose (filled symbol) of ^{125}I-HbV to hemorrhagic shock rats at a dose of 1,400 mg Hb/kg for each injection. Each point represents the mean ± SD (n=5). Plasma concentration percentage profile for the first dose (○) was obtained from injection of a dose of ^{125}I-HbV administered after hemorrhagic shock. The profile for the second dose (•) was obtained from the injection of a dose of ^{125}I-HbV 1 hour after injection of the first dose of nonradiolabeled HbV administered after hemorrhagic shock. (B) Determination of IgM against HbV 5 days after a single intravenous injection of HbV to normal rats at a dose of 0.1 mg Hb/kg (closed bars) or 1 hour after a single intravenous injection of HbV to hemorrhagic shock rats at a dose of 1,400 mg Hb/kg (open bars) in mice. IgM against HbV were detected by ELISA. Each bar represents the mean ± SD (n=3–5).